Geoscience Frontiers 12 (2021) 101118

HOSTED BY

Contents lists available at ScienceDirect

Geoscience Frontiers

journal homepage: www.elsevier.com/locate/gsf

Research Paper

PGE and isotopic characteristics of Shergol and Suru Valley Ophiolites, Western Ladakh: Implications for supra-subduction tectonics along Indus Suture Zone

Irfan Maqbool Bhat [a,*], Talat Ahmad [b], D.V. Subba Rao [c], Srinivasan Balakrishnan [d], N.V. Chalapathi Rao [e]

[a] Department of Earth Sciences, University of Kashmir, Srinagar 190006, India
[b] Vice Chancellors Office, University of Kashmir, Srinagar 190006, India
[c] Geochemistry Division, CSIR-National Geophysical Research Institute (NGRI), Hyderabad 500007, India
[d] Department of Earth Sciences, Pondicherry University, Puducherry 605014, India
[e] Centre of Advanced Study in Geology, Institute of Science, Banaras Hindu University, Varanasi 221005, India

ARTICLE INFO

Article history:
Received 19 December 2019
Received in revised form 10 September 2021
Accepted 20 November 2021
Available online 24 December 2020

Handling Editor: S. Ganguly

Keywords:
PGE
Nd-isotope
Mantle peridotites
Ophiolites
Ladakh
Neo-Tethys Ocean

ABSTRACT

Present study reports the PGE-geochemistry of mantle peridotites and Nd-isotope geochemistry of arc related mafic rocks from the Indus Suture Zone (ISZ), western Ladakh. The total PGE concentration of the Shergol and Suru Valley peridotites ($\sum$PGE = 96–180 ppb) is much higher than that of the primitive mantle and global ophiolitic mantle peridotites. The studied peridotites show concave upward PGE-distribution patterns with higher palladium-group PGE/Iridium-group PGE ratios (i.e., 0.8–2.9) suggesting that the partial melting is not the sole factor responsible for the evolution of these peridotites. The observed PGE-distribution patterns are distinct from residual/refractory mantle peridotites, which have concave downward or flat PGE-distribution patterns. Relative enrichment of palladium-group PGE as well as other whole-rock incompatible elements (e.g., LILE and LREE) and higher Pd/Ir ratio (1.1–5.9) reflects that these peridotites have experienced fluid/melt interaction in a supra-subduction zone (SSZ) tectonic setting. Also, the Shergol mafic intrusives and Dras mafic volcanics, associated with the studied peridotites, have high $^{143}Nd/^{144}Nd$ ratios (i.e., 0.512908–0.513078 and 0.512901–0.512977, respectively) and positive $\varepsilon_{Nd(t)}$ (calculated for t = 140 Ma) values (i.e., +5.3 to +8.6 and + 5.1 to +6.6, respectively), indicating derivation from depleted mantle sources within an intra-oceanic arc setting, similar to Spongtang and Nidar ophiolites from other parts of Ladakh Himalaya. The transition from SSZ-type Shergol and Suru Valley peridotites to Early Cretaceous tholeiitic Shergol mafic intrusives followed by tholeiitic to calc-alkaline Dras mafic volcanics within the Neo-Tethys Ocean exhibit characteristics of subduction initiation mechanism analogous to the Izu-Bonin-Mariana arc system within western Pacific.

1. Introduction

Ophiolites represent the slivers of ancient oceanic lithosphere, characterized by refractory mantle peridotites, ultramafic-mafic plutonic rocks, sheeted dyke complex, volcanic extrusives and sedimentary rock units that collectively preserve comprehensive record of magmatic and tectonic processes associated with the opening and destruction of ocean basins (Coleman, 1977; Shervais, 2001; Pearce, 2003; Dilek and Furnes, 2011; Saccani, 2015). The geochemical studies on residual mantle peridotites from ophiolites are vital in understanding various pre and post-melting mantle processes such as., mantle heterogeneity, melting and melt extraction processes, mantle wedge metasomatism, seafloor weathering and serpentinization (Kelemen et al., 1992; Bodinier and Godard, 2003; Canil, 2004; Niu, 2004; Ishikawa et al., 2007; Piccardo et al., 2007; Deschamps et al., 2013; Pal et al., 2014). Compared to extensively studied mid-ocean ridge ophiolite peridotites (Niu, 2004; Singh et al., 2013; Bhat et al., 2017; Ao et al., 2020), the supra-subduction zone (SSZ) ophiolite peridotites attracted substantial consideration as they include fore-arc, arc and back-arc peridotites corresponding to processes of fore-arc extension, arc development and back-arc spreading, respectively (Leat et al., 2004; Arai et al., 2006; Aldanmaz et al., 2008; Rollinson and Adetunji, 2013; Arai and Miura, 2016; Qian et al., 2020; Ullah et al., 2020). Therefore, the SSZ peridotites are imperative in understanding the extent of fluid/melt interaction in the mantle wedge during pre and post-melting episodes (Parkinson and Pearce, 1998; Dai et al., 2011; Moghadam et al., 2014).

The Platinum Group Elements (PGE) consist of two groups; the iridium-group PGE i.e., IPGE including Ir, Os and Ru which are siderophile and refractory in nature whereas, the palladium-group

* Corresponding author.
E-mail address: imbhat89@gmail.com (I.M. Bhat).

https://doi.org/10.1016/j.gsf.2020.11.014

PGE i.e., PPGE including Rh, Pt and Pd are chalcophile and volatile in nature. In crustal magmatic rocks, PGE abundances are extensively utilized to understand the various magmatic processes (Rollinson, 1993; Lorand et al., 2003, 2008; Crocket et al., 2013; Saha et al., 2018; Fu et al., 2019). Having highly siderophile and chalcophile nature, they are efficiently fractionated into the Earth's core and mantle, leaving the crust strongly depleted in PGE (Naldrett and Duke, 1980). PGE have always attracted worldwide attention as important exploration target. In fact, many earlier studies on PGE were inspired by the metal potential of large layered intrusion e.g., Bushveld Complex (Alard et al., 2000), and Large Igneous Province (LIP), such as the Permo-Triassic Siberian LIP (Brugmann et al., 1993) and Emeishan LIP, SW China (Song et al., 2009). Presently, the PGE mineralization is targeted in greenstone belt associated basalts, komatiites, chromitites (Manikyamba and Saha, 2014; Saha et al., 2015; Singh et al., 2016; Mondala et al., 2019), and ophiolite related rocks (Dai et al., 2011; Uysal et al., 2012; Singh et al., 2013; Qiang et al., 2015; Fu et al., 2019; Ullah et al., 2020).

Ophiolites along the Indus Suture Zone (ISZ) are not only important for understanding the India-Eurasia collision history, but they may also contain economic mineral deposits in the form of podiform chromites, noble metal alloys (PGE and Au) and Ni-Cu-sulfides. The Shergol and Suru Valley ophiolitic slices represent dismembered ophiolites along the ISZ, exposed respectively at Shergol Village and Suru Valley in the Kargil district of western Ladakh. Earlier whole-rock (major and trace element data) and mineral (major element data) geochemistry of the Shergol and Suru Valley ophiolitic slices, along the ISZ, Ladakh Himalaya have been studied to understand petrogenesis and tectonic setting (Bhat et al., 2017, 2019a, 2019b) however, no PGE and isotope geochemistry have been considered so far. This study addresses the PGE geochemistry of the Shergol and Suru Valley ophiolitic peridotites, and Nd-isotope geochemistry of the mafic rocks viz. Shergol mafic intrusives and Dras mafic volcanics along the ISZ, western Ladakh. Our results provide insights into: (1) the intra-oceanic subduction initiation within the Neo-Tethys Ocean, (2) source metasomatism, and (3) melt-rock interaction in a subduction zone setting.

2. Geological setting

The Cenozoic closure of the Neo-Tethys Ocean followed by the subsequent collision of Afro-Arabian-Indian plate towards south with Eurasian plate towards north is responsible for the growth of the Alpine-Himalayan mountain system (Molnar and Tapponnier, 1975; Yin and Harrison, 2000; Dilek and Furnes, 2009), and the subsequent evolution of the Tethyan ophiolite belt (Moores et al., 2000; Dilek and Furnes, 2011; Ghosh et al., 2017). The Tethyan ophiolite belt along the Alpine-Himalayan mountain system extends westwards from Alps, Greece and Turkey, through Iran, Oman, Afghanistan, Pakistan, India, Tibet, Nagaland-Manipur towards Andaman-Nicobar Islands and Indonesia eastwards (Barth et al., 2008; Saha et al., 2010; Khogenkumar et al., 2016; Singh et al., 2017; Ao et al., 2020; Ullah et al., 2020).

The ISZ, representing the suture zone between Indian and Eurasian plates, forms the central part of the Alpine-Himalayan mountain system and comprises different tectono-stratigraphic units from south to north; Lamayuru Complex, ophiolitic melange, Dras arc complex, Indus Formation and Ladakh batholith (Bhat et al., 2019a, and references therein). Previous studies have recorded occurrences of ophiolites, classified as Tethyan type ophiolites by Moores et al. (2000), in several parts of Ladakh along the ISZ (Fig. 1a), representing both ideal and dismembered ophiolite sequences comprising basal residual mantle peridotites, ultramafic-mafic cumulates, isotropic gabbros, dolerite dykes and basic volcanics interlayered with sedimentary rocks (Gansser, 1964, 1980; Frank et al., 1977; Honegger et al., 1982; Searle et al., 1987; Ahmad et al., 1996, 2008; Robertson, 2000; Corfield et al., 2001; Maheo et al., 2004). They occur as discrete slices along the ISZ (Brookfield and Reynolds, 1981; Thakur and Misra, 1984; Chatterjee et al., 2013) and from south-east to north-west are; Nidar ophiolite (Maheo et al., 2004; Ahmad et al., 2008), Spongtang ophiolite (Clift et al., 2002; Buckman et al., 2018), Shergol ophiolitic slice (Sinha and Mishra, 1992; Bhat et al., 2017), Suru Valley ophiolitic slice (Reuber, 1989; Robertson, 2000; Bhat et al., 2019b) and Dras-Thasgam ophiolitic slice (Radhakrishna et al., 1984; Radhakrishna et al., 1987; Bhat et al., 2019a). The published geochronological data corresponds to Early Jurassic to Mid-Cretaceous age for these ophiolitic slices e.g., U-Pb zircon age of Dras-Kargil Granodiorite (103 ± 3 Ma; Honegger et al., 1982), K-Ar age of primary green hornblende from Thasgam gabbro (~157 ± 7 Ma; Reuber et al., 1990), $^{40}Ar/^{39}Ar$ age of amphibole from Nidar gabbro (~120 Ma; Maheo et al., 2004), Sm-Nd mineral and whole-rock age of Nidar ophiolite (~140 ± 32 Ma; Ahmad et al., 2008), U-Pb zircon age of Spongtang diorite ~177 ± 1 Ma and andesite ~88 ± 5 Ma (Pedersen et al., 2001) and U-Pb SHRIMP zircon age of Spongtang gabbro (~136 ± 1 Ma; Buckman et al., 2018).

The Shergol ophiolitic slice forms one of the major lithological unit of the Sapi-Shergol ophiolitic melange (Fig. 1b), dominantly comprising serpentinized peridotites (i.e., Shergol peridotites of Bhat et al., 2017) in association with Shergol mafic intrusives/gabbros. These fine to medium grained mafic intrusives also occur as individual blocks in pelagic sediments near Shergol Village and generally show light color weathered surfaces at the outcrop. According to Reuber (1989), the Suru Valley ophiolitic slice (Fig. 1b), represent tectonically disrupted oceanic substratum of the Cretaceous Dras arc complex, dominantly comprising serpentinized peridotites (i.e., Suru Valley peridotites of Bhat et al., 2019b) with minor gabbros. Also, the Dras mafic volcanics (or Dras-I volcanic Formation of Reuber, 1989), represent a dominant lithological unit of Dras arc complex, best exposed along Dras-Leh National Highway from Dras to Kargil (Radhakrishna et al., 1984; Reuber, 1989). The Dras arc complex near Dras area is composed of basaltic flows intercalated with volcano-clastic sediments, Radiolarian chert and Orbitolina limestone (Honegger et al., 1982).

3. Sampling and petrography

For the present study, ten samples of Shergol and Suru Valley peridotites, ten samples of Shergol mafic intrusives and six samples of Dras mafic volcanics were collected from the selected locations as shown on map (Fig. 1b). The Shergol and Suru Valley ophiolite peridotite samples are serpentinized to varying degrees and are characterized by inter-penetrating, mesh and pseudomorphic textures (Fig. 2a and b). Petrographically, their mineral assemblage includes up to 60 vol% serpentine after olivine and < 35 vol% bastites after orthopyroxene besides, < 10 vol% clinopyroxene, partly altered red-brown spinel and fine-grained magnetite (Fig. 2a and b). Based on mineral assemblages these peridotites were classified as spinel bearing harzburgites (Bhat et al., 2019b). The orthopyroxene and clinopyroxene mostly occur as large crystals (0.5 to 1 mm) with subhedral granular shape against the fine-grained serpentine matrix, besides, some olivine relics (< 0.2 mm in size) in orthopyroxene were also observed in few samples (Fig. 2a). Also, serpentine, chlorite and magnetite are the main metamorphic products after primary phases. The subhedral to euhedral shaped spinel grains of <1 mm size are ubiquitously oxidized to magnetite along grain boundaries and fractures (Fig. 2b). Back scattered electron (BSE) images of spinel grains (Fig. 2c and d) reveal zoning with core of Cr-spinel mantled by thin rim of magnetite (Fig. 2c). Also, electron probe micro analysis (EPMA) reveal traces of sulfide grains in the form of pentlandite (an ore of Ni) of <0.1 mm size, enclosed within Cr-spinel grains of the studied peridotites (Fig. 2d).

The Shergol mafic intrusives are fine to medium grained, display uniform mineral assemblages, dominantly composed of lath shaped plagioclase (0.1–0.5 mm size) and embayed clinopyroxene (0.2–1 mm size) in equigranular to sub-ophitic textural relationship with minor iron oxide (Fig. 2e). Besides, sericite, chlorite and amphibole are present as metamorphic mineral assemblage. In terms of modal abundance, the

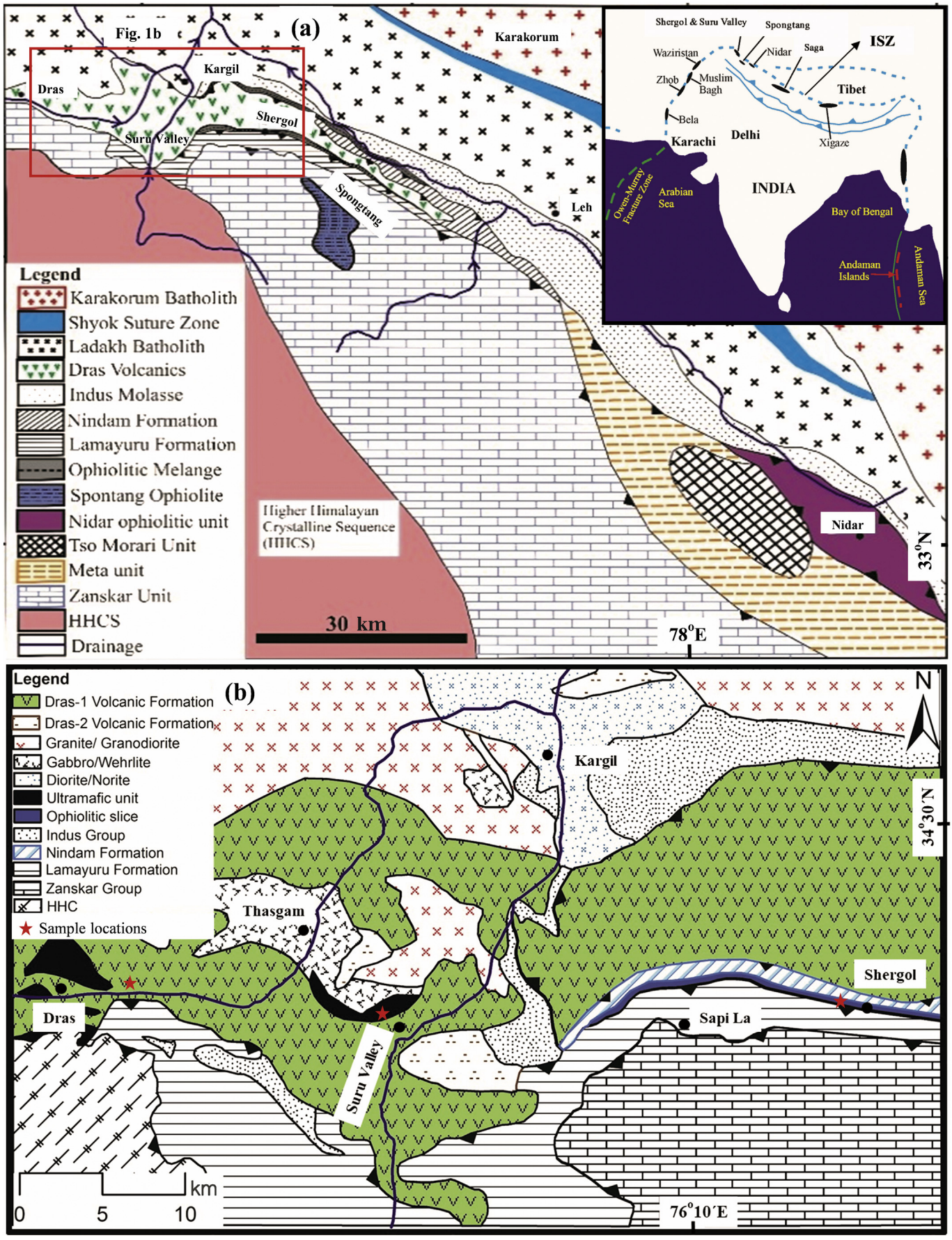

Fig. 1. (a) Geological map of Ladakh Himalaya modified after Maheo et al. (2004), also showing at top right distribution of Neo-Tethyan ophiolites along the Indus Suture Zone (ISZ) after Dilek and Furnes (2009), and (b) geological map of Kargil district, Ladakh showing study are and sample locations (modified after Reuber, 1989).

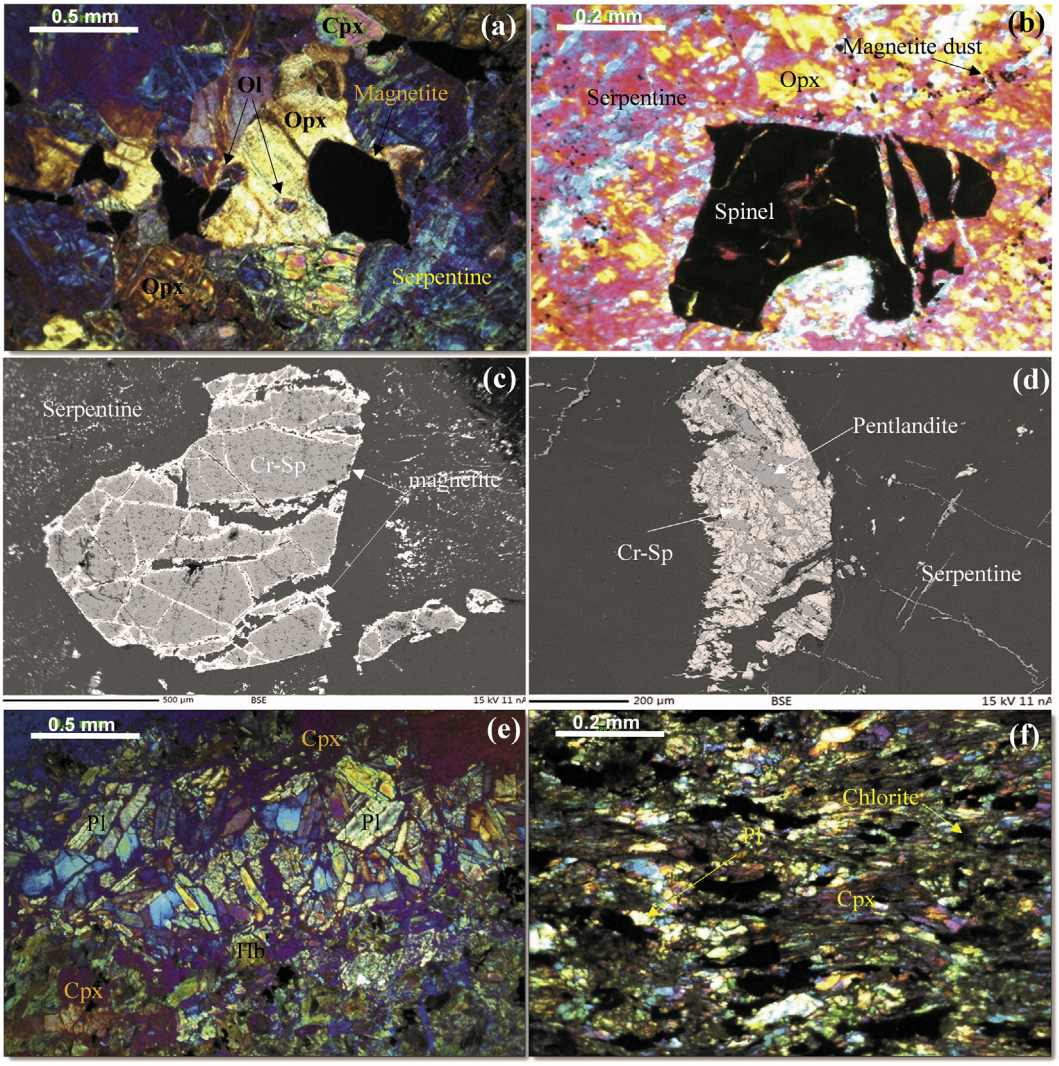

Fig. 2. Representative photomicrographs (under crossed polarized light) and back scattered electron (BSE) images of studied rock types: (a) photomicrograph of a peridotite with olivine (Ol) relicts in orthopyroxene (Opx), rare clinopyroxene (Cpx) and magnetite surrounded by a serpentine groundmass, (b) photomicrograph of a peridotite with corroded and fractured subhedral red-brown spinel grain besides, orthopyroxene (Opx) and magnetite suspended in a serpentine groundmass, (c) BSE-image of a subhedral spinel grain with Cr-spinel (Cr-Sp) core rimmed by a thin film of magnetite in a serpentine groundmass, (d) BSE-image of a subhedral pentlandite grains associated with Cr-Sp grain in a serpentine matrix, (e) photomicrograph of a Shergol mafic intrusive (i.e., gabbro) with plagioclase (Pl) and clinopyroxene (Cpx) showing intersertal to sub-ophitic texture, also hornblende (Hb) and oxide is present, and (f) photomicrograph of a Dras mafic volcanic (i.e., basalt) showing oriented grains of plagioclase (Pl), clinopyroxene (Cpx) and chlorite with some oxides.

Shergol mafic intrusives have 70 vol%–65 vol% plagioclase, 30 vol%–25 vol% clinopyroxene and < 5 vol% oxide, amphibole and chlorite (Bhat et al., 2019c). Also, the Dras mafic volcanics are fine to medium grained, dominantly composed of augite (< 0.2 mm size) and plagioclase (0.1–0.2 mm size) as phenocrysts, embedded in a groundmass composed of plagioclase, pyroxene and minor iron oxide. The constituent mineral assemblage shows porphyritic, intergranular and ophitic textural relationship (Fig. 2f). Petrographically, the Dras mafic volcanics are classified as basalts characterized by low-grade metamorphic mineral assemblage of chlorite and minor epidote (Bhat et al., 2019a).

4. Analytical techniques

The representative peridotite samples collected for PGE analysis were first examined under transmitted light microscopy equipped with imaging facility at the Department of Earth Sciences, University of Kashmir. The minute pentlandite crystals were analyzed using Electron Probe Micro Analyzer (EPMA) CAMECA SX-Five Instrument, operating at an accelerating voltage of 15 kV and probe current of 40 nA, at the Banaras Hindu University, Varanasi, India. Quality control was maintained by analyzing well-calibrated natural mineral standards (e.g., chromite for Cr and hematite for Fe) during each electron microprobe session. Routine X-ray spectral analysis (calibration, acquisition, quantification) and data processing were carried out using SxSAB version 6.1 software of CAMECA and repeated analyses of individual points show analytical error of <2%.

PGE concentrations were analyzed using the nickel sulphide (NiS) fire-assay pre-concentration technique described by Balaram (2008). The prepared sample solution was analyzed by HR-ICP-MS at CSIR-NGRI, Hyderabad, India. CANMET PGE reference materials WMS-1 (i.e., massive sulphide) and WMG-1 (i.e., mineralized gabbro) were used as an external standard possessing all PGE certified values (Balaram, 2008 and references therein). The detection limits obtained range from 0.003 to 0.024 ppb for different PGE. The precision for six-replicate measurements of the raw counts was <3% RSD for PGE and Au. Precision and accuracy of WMS-1 and WMG-1 used as international reference materials are referred to Manikyamba and Saha (2014). For isotopic analysis, 50 to 150 mg sample powder of Shergol mafic

Table 1
Mineral chemistry of pentlandite from Shergol ophiolitic peridotites, western Ladakh.

ID	Cobalt Pentlandite								Pentlandite				
	TDP2		TDP7		TDP8		TDP9			TDP2		TDP8	
Point	P-13	P-15	P-17	P-25	P-44	P-45	P-49	P-50	Point	P-42	P-48	P-22	P-27
Fe	25.81	25.56	25.99	26.33	26.82	25.76	27.01	26.64	Fe	1.56	1.81	1.38	1.78
Ni	35.43	35.95	35.55	34.86	33.91	34.01	34.41	34.63	Ni	63.77	63.08	64.05	63.38
S	32.93	32.61	32.72	32.81	32.96	33.31	32.85	32.86	S	34.24	34.96	34.86	34.05
Co	5.54	5.58	5.37	5.39	5.69	6.78	5.34	5.56	Co	–	–	–	–
Total (wt.%)	99.71	99.69	99.63	99.38	99.38	99.86	99.62	99.68	Total (wt.%)	99.57	99.84	100.29	99.21

intrusives and Dras mafic volcanics were digested using double-distilled acids e.g., HF, HCl and HNO_3 in different proportions and were measured using Thermal Ionization Mass Spectrometer (TIMS, Thermo-Finnigan, Model-Triton) at the Department of Earth Sciences, Pondicherry University, Puducherry, India. Sample dissolution procedure and other analytical details (i.e., precision and accuracy of BCR-2, used as reference material) for Nd-isotope analysis are same as described by Kingson et al. (2017). The detailed sample dissolution procedure for PGE and isotope analysis is described in Supplementary File.

5. Geochemistry

5.1. Mineral geochemistry

Detailed petrographic and scanning electron microscope (SEM) examination of polished thin sections of the studied peridotites could not locate discrete PGE minerals down to 2 μm scale. However, EPMA studies reveal traces of sulfides in the form of pentlandite grains of <100 μm across, associated with spinel grains in the Shergol ophiolitic peridotites (Fig. 2d). The mineral chemistry data of pentlandite from Shergol ophiolitic peridotites is given in Table 1. The composition of pentlandite is $(Ni_{63-64}\ Fe_{1-2})S_{34-35}$ while, cobalt pentlandite is $(Ni_{34-36}\ Fe_{26-27}\ Co_{5-7})S_{32-33}$. Also, according to Bhat et al. (2019b), the studied peridotites are characterized by primary Cr-rich spinels (with Cr_2O_3 = 35.1 wt.%–43.4 wt.% and Al_2O_3 = 22.4 wt.%–30.4 wt.%) and highly magnesian olivines (Fo_{90-92}) and orthopyroxenes ($En_{91-93}\ Fs_{6.4-8.7}$) comparable to SSZ-peridotites (Parlak et al., 2020).

5.2. Whole-rock geochemistry

Whole-rock major and trace element compositions of the Dras mafic volcanics, Shergol and Suru Valley peridotites and Shergol mafic intrusives were previously studied and reported by Bhat et al. (2017, 2019a, 2019b, 2019c) and therefore are not described here in detail. For Shergol and Suru Valley peridotites, the major and trace element compositions discussed here are summarized in Supplementary Table S1 while, for Dras mafic volcanics and Shergol mafic intrusives in Supplementary Table S2. The studied peridotite samples have low to moderate loss on ignition (LOI) values (3 wt.%–12 wt.%) owing to moderate degree serpentinization. These peridotites are characterized by higher magnesium number ($Mg\# = Mg^{2+}/[Mg^{2+} + Fe^{2+}] \times 100$) of 90–92, Cr (2362–4728 ppm) and Ni (1868–3230 ppm) as compared to primitive mantle (PM) i.e., 89.3 ppm, 2625 ppm and 1960 ppm, respectively, besides, lower concentration of incompatible elements e.g., Al_2O_3 (1.8–2.9 anhydrous wt.%) and CaO (0.03–1.5 anhydrous wt.%) and U-shaped REE-patterns. Similarly, the Dras mafic volcanics and Shergol mafic intrusives have very low LOI values (< 2.5 wt.%) indicating least secondary alteration of constituent elements and are respectively characterized by whole-rock Mg# (57–68 and 56–73), SiO_2 (46–53 wt.% and 46–52 wt.%), Al_2O_3 (12.4–15.3 wt.% and 12–15.5 wt.%), TiO_2 (0.7–1.1 wt.% and 0.14–1.3 wt.%), CaO (8–16.4 wt.% and 7–16.8 wt.%), Cr (104–278 ppm and 69–511 ppm) and Ni (153–225 ppm and 60–299 ppm). In MgO/SiO_2 versus Al_2O_3/SiO_2 plot (Fig. 3), the studied peridotite samples have lower Al_2O_3/SiO_2 ratios than PM similar to residual peridotites whereas, Dras mafic volcanics and Shergol mafic intrusives have higher ratios analogous to derivative melts.

The normal mid ocean ridge basalt (NMORB) normalized multi-element patterns of the studied peridotites (Fig. 4a) and the studied mafic rocks (Fig. 4b) exhibit subparallel coherent trends with enriched large-ion lithophile element (LILE; Rb, Ba, K, Pb and Sr) and depleted high field-strength element (HFSE, e.g., Nb and Ti in peridotites while Nb, P, Zr and Ti in mafic rocks) signatures compared to other trace elements. These geochemical characteristics are analogous to subduction zone magmas (Shervais, 2001).

5.3. PGE geochemistry of peridotites

The PGE (including Au) data of the studied peridotite samples is given in Table 2. The total PGE (excluding Au) contents of the Shergol and Suru Valley peridotites are higher (i.e., > 96 ppb, and vary from 96 to 180 ppb with an average of 138 ppb) than PM (i.e., 23.5 ppb; after McDonough and Sun, 1995). The PPGE and IPGE abundances in the studied peridotites range from 56 to 122 ppb and 34–83 ppb, respectively while, Pt-anomaly i.e., Pt/Pt* ratio $[=Pt_N/(Rh_N \times Pd_N)^{1/2}$ where "N" represents PM normalization] ranges from 0.5–0.8. The negative Pt-anomaly is a consequence of relative extraction of Pt-alloys as compared to Rh and Pd from mantle residue (Garuti et al., 1997; Kepezhinskas et al., 2002; Zheng et al., 2004). Similarly, the Au concentration of these peridotites ranges from 40 to 91 ppb and is 40–90 times higher that of PM (i.e., 1 ppb; after McDonough and Sun (1995) and other Neo-Tethyan ophiolitic peridotites (Singh et al., 2013)). However, present Au concentration is comparable to tectonite peridotites from Nagaland-Manipur ophiolite complex (i.e., 11–77 ppb; after

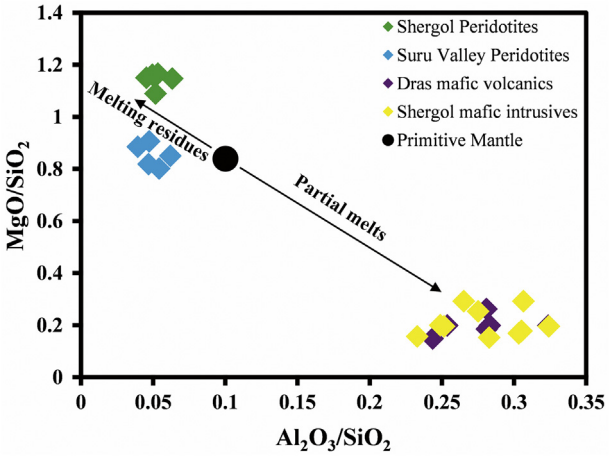

Fig. 3. Plot of bulk-rock anhydrous MgO/SiO_2 versus Al_2O_3/SiO_2 of the Shergol and Suru Valley peridotites in comparison with Shergol mafic intrusives and Dras mafic volcanics. The compositional variation expected during partial melting is shown with arrows. Estimated primitive mantle compositions are after McDonough and Sun (1995).

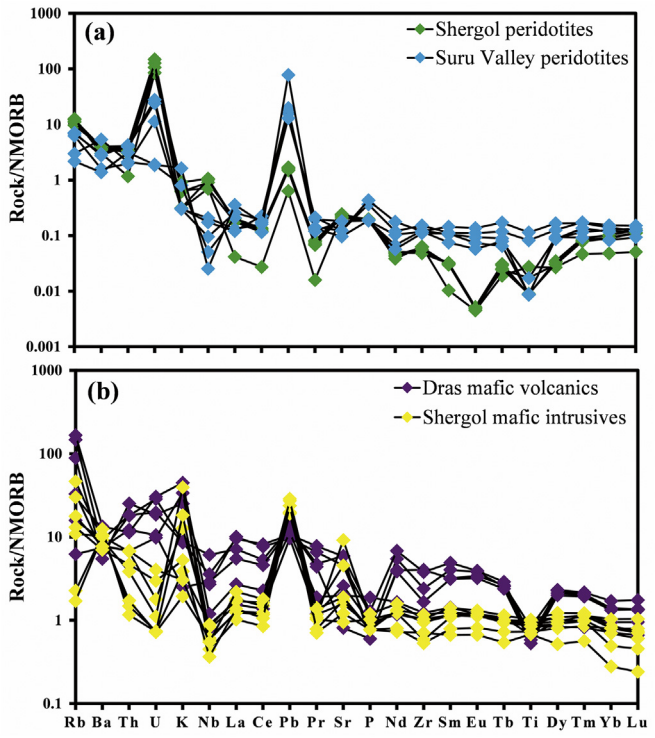

Fig. 4. NMORB normalized multi-element spidergram of: (a) Shergol and Suru Valley peridotites, and (b) Shergol mafic intrusives and Dras mafic volcanics. Normalizing values are after McDonough and Sun (1995).

Singh et al., 2017). Also, in the studied peridotites, the various chondrite normalized PGE ratios such as, $(Pd/Ir)_N$, $(Pd/Pt)_N$, $(Pd/Ru)_N$, $(Os/Ir)_N$, and $(Ru/Ir)_N$ are respectively (1–4.9), (1.1–2.4), (1.1–3.5), (0.9–1.5), and (1–1.7) (chondrite values after McDonough and Sun, 1995).

Also, the PM normalized PGE-patterns of the studied peridotites are plotted in order of increasing incompatibility from left to right (Fig. 5; normalization values are after McDonough and Sun, 1995). Fields of Nidar chromitites (after Siddaiah and Masuda, 2001) and Mesozoic Neo-Tethyan ophiolites (after Singh et al., 2013 and references therein) are

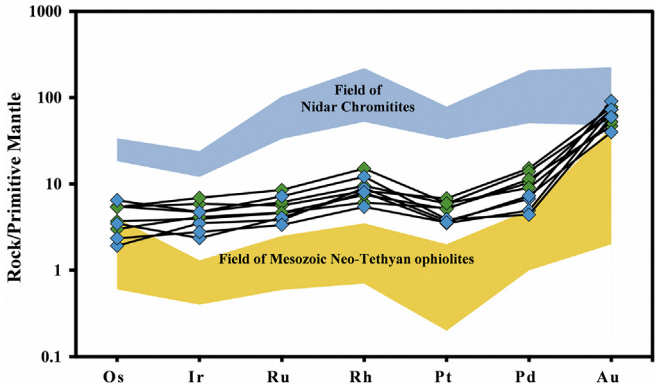

Fig. 5. PM-normalized PGE-patterns of the Shergol and Suru Valley ophiolite peridotites in comparison to Mesozoic Neo-Tethyan ophiolite peridotites (data after Singh et al., 2013) and Nidar Chromitites, eastern Ladakh (data after Siddaiah and Masuda, 2001). Normalizing values are after McDonough and Sun (1995).

shown for comparison. It is evident from the figure that the PGE distribution patterns are consistent with nearly flat patterns from Os to Pt and positive slope from Pt to Au, reflecting concave upward PGE distribution patterns.

5.4. Nd-Isotope geochemistry of mafic rocks

The whole rock Nd-isotope data of the Dras mafic volcanics and Shergol mafic intrusives is listed in Table 3. The $^{143}Nd/^{144}Nd$ ratio of the Shergol mafic intrusives and Dras mafic volcanics varies from 0.512908 to 0.513078 and 0.512901 to 0.512977, respectively. Similarly, the $\varepsilon_{Nd}(t)$(calculated for $t = 140$ Ma) of the Shergol mafic intrusives and Dras mafic volcanics is positive and respectively ranges from +5.3 to +8.6 and + 5.1 to +6.6.

6. Discussion

6.1. Alteration effects on PGE geochemistry

Previous studies have shown some degree of PGE mobility in ophiolite mantle peridotites (e.g., Yu et al., 2001; Zaccarini et al., 2011, 2018) and

Table 2
PGE concentration (in ppb) in Shergol and Suru Valley ophiolitic peridotites, western Ladakh.

ID	Shergol Peridotites						Suru Valley Peridotites				WMG-1		
	SHP6	TDP2	TDP7	TDP8	TDP9	SP5	SP7	SP8	DP3	DP5	OV	CV	%RSD
Ru	28.21	30.78	23.09	23.32	42.53	19.15	20.38	36.01	16.78	22.54	34.3	35 ± 5	2
Rh	7.46	8.55	5.49	6.75	13.56	12.03	12.2	11.93	11.53	10.06	25.6	24 ± 2	1.3
Pd	58.09	54.51	40.3	44.1	35.17	26.42	19.28	17.18	28.45	60.47	375.1	382 ± 13	1.8
Os	18.38	18.63	12.56	10.23	18.35	6.53	11.82	16.99	7.98	9.37	–	–	–
Ir	18.84	15.09	12.63	13.28	22.1	11.25	7.54	15.15	8.89	10.16	45.3	46 ± 4	1.6
Pt	48.28	42.06	37.27	36.48	42.32	26.51	24.92	27.73	25.44	51.15	727.2	731 ± 35	2.9
∑PGE	180.3	169.6	131.3	134.2	174	101.9	96.1	124.9	99.1	163.8	–	–	–
Au	77.79	62.26	72.5	47.03	52.49	91.15	72.8	59.75	39.88	69.57	109.6	110 ± 17	1.5
Pt/Pt*	0.74	0.62	0.8	0.68	0.62	0.48	0.52	0.62	0.45	0.69	–	–	–
IPGE	65.4	64.5	48.3	46.8	82.9	36.9	39.7	68.2	33.7	42.1	–	–	–
PPGE	114.8	105.1	83.1	87.3	91.1	64.96	56.4	56.8	65.4	121.7	–	–	–
PPGE/IPGE	1.76	1.63	1.72	1.86	1.10	1.76	1.42	0.83	1.94	2.89	–	–	–
Pd/Ir	3.14	3.61	3.19	3.32	1.59	2.35	2.56	1.13	3.2	5.9	–	–	–
Pd/Ru	2.09	1.77	1.75	1.89	0.83	1.38	0.95	0.48	1.7	2.68	–	–	–
Pd/Rh	7.92	6.38	7.34	6.53	2.59	2.2	1.58	1.44	2.47	6.01	–	–	–
Pd/Pt	1.22	1.30	1.08	1.21	0.83	1	0.77	0.62	1.12	1.18	–	–	–
Ru/Pt	0.58	0.73	0.62	0.64	1	0.72	0.82	1.3	0.66	0.44	–	–	–
Os/Ir	0.98	1.23	0.99	0.77	0.83	0.58	1.57	1.45	0.9	0.92	–	–	–
Ru/Ir	1.50	2.04	1.83	1.76	1.92	1.7	2.7	2.38	1.89	2.22	–	–	–
Pt/Pd	0.82	0.77	0.92	0.83	1.2	1	1.29	1.61	0.89	0.85	–	–	–
Cu/Pd	859	1432	1869	1573	1847	1164	1683	1939	1029	360	–	–	–

Footnote: *$Pt/Pt^* [Pt_N/(Rh_N \times Pd_N)^{1/2}]$ normalized to primitive mantle after McDonough and Sun (1995).*
The observed PGE values (OV) of the reference material WMG-1 (averaged after six replicate analysis) are compared with certified values (CV) after Balaram (2008 and references therein).

Table 3
Nd isotope data of Dras mafic volcanics (DM) and Shergol mafic intrusives (SM) from western Ladakh. The error (1σ) in ratios is at the last decimal place.

ID	Rock Type	Nd (ppm)	$^{143}Nd/^{144}Nd$	1σ SD	$\varepsilon_{Nd}(t)$ (t = 140 Ma)
DM9	Dras mafic volcanic	39.89	0.512901	0.0000037	+5.1
DM10	Dras mafic volcanic	29.22	0.512934	0.0000028	+5.8
DM11	Dras mafic volcanic	49.74	0.512921	0.0000019	+5.5
DM21	Dras mafic volcanic	28.11	0.512977	0.0000051	+6.6
DM28	Dras mafic volcanic	8.54	0.512964	0.0000023	+6.4
DM31	Dras mafic volcanic	12.08	0.512924	0.0000025	+5.6
SM1	Shergol mafic intrusive	9.46	0.512960	0.0000025	+6.3
SM7	Shergol mafic intrusive	5.84	0.512944	0.0000021	+6.0
SM6	Shergol mafic intrusive	8.91	0.513045	0.000005	+7.9
SM11	Shergol mafic intrusive	11.49	0.513075	0.0000027	+8.5
SM24	Shergol mafic intrusive	8.85	0.513078	0.0000021	+8.6
SM26	Shergol mafic intrusive	5.31	0.512969	0.0000023	+6.5
SM28	Shergol mafic intrusive	9.68	0.512986	0.000002	+6.8
SM14	Shergol mafic intrusive	6.23	0.512908	0.0000024	+5.3
SM17	Shergol mafic intrusive	11.62	0.512978	0.0000024	+6.6
SM19	Shergol mafic intrusive	10.53	0.512940	0.0000034	+6.0

Neoarchean greenstone belts (Goldfarb et al., 2005; Saha et al., 2015). The mobility of PGE in mantle peridotites is controlled by their solubility in metamorphic fluids and the stability of the host mineralogy (e.g., sulfides) during secondary alteration processes (Pan and Wood, 1994; Said et al., 2011). According to Hanley et al. (2008), Pd, Pt and Au display variable degrees of mobility, however, the other PGE are relatively least mobile.

Replacement of primary igneous minerals by metamorphic assemblage due to serpentinization is extensive in the global mantle peridotites (Bodinier and Godard, 2003; Niu, 2004; Deschamps et al., 2010, 2013; Xu et al., 2020). This is manifested by increased LOI values in the studied peridotites however, has little effect on the relative abundances of majority of major and trace elements (Bhat et al., 2017, 2019b). As reported earlier, the ophiolite belt along the ISZ has undergone greenschist to amphibolite grade of metamorphism (Sinha and Mishra, 1992; Singh et al., 2013), which might have triggered some PGE mobility via bisulfide complexes (Gammons et al., 1992) in the studied peridotites. Therefore, in order to check the PGE mobility in Shergol and Suru Valley peridotites, we have plotted PGE against whole-rock LOI values (Fig. 6). In this figure, all the PGE exhibit no correlation with LOI values, reflecting their least mobility. Thus, the PGE geochemistry of the studied peridotites can be used for petrogenetic interpretation.

6.2. PGE fractionation and mantle melting

In mantle peridotites, PGE distribution is controlled by various factors such as; lateral geochemical heterogeneity (Singh et al., 2018), partial melting history and sulphide saturation of the upper mantle (Zhou et al., 2005; Lorand et al., 2008; Uysal et al., 2012), mantle metasomatism (Lorand et al., 1993; Yu et al., 2001), and secondary alteration (Said et al., 2011). The observed higher MgO/SiO_2 ratio while lower Al_2O_3/SiO_2 ratio (Fig. 3), depleted HFSE e.g., Nb and Ti, and enriched mantle compatible elements e.g., Mg, Fe, Ni, Cr, and Cu reflects that the studied peridotites have refractory/residual nature analogous to SSZ peridotites (Bodinier and Godard, 2003; Xu and Liu, 2019;

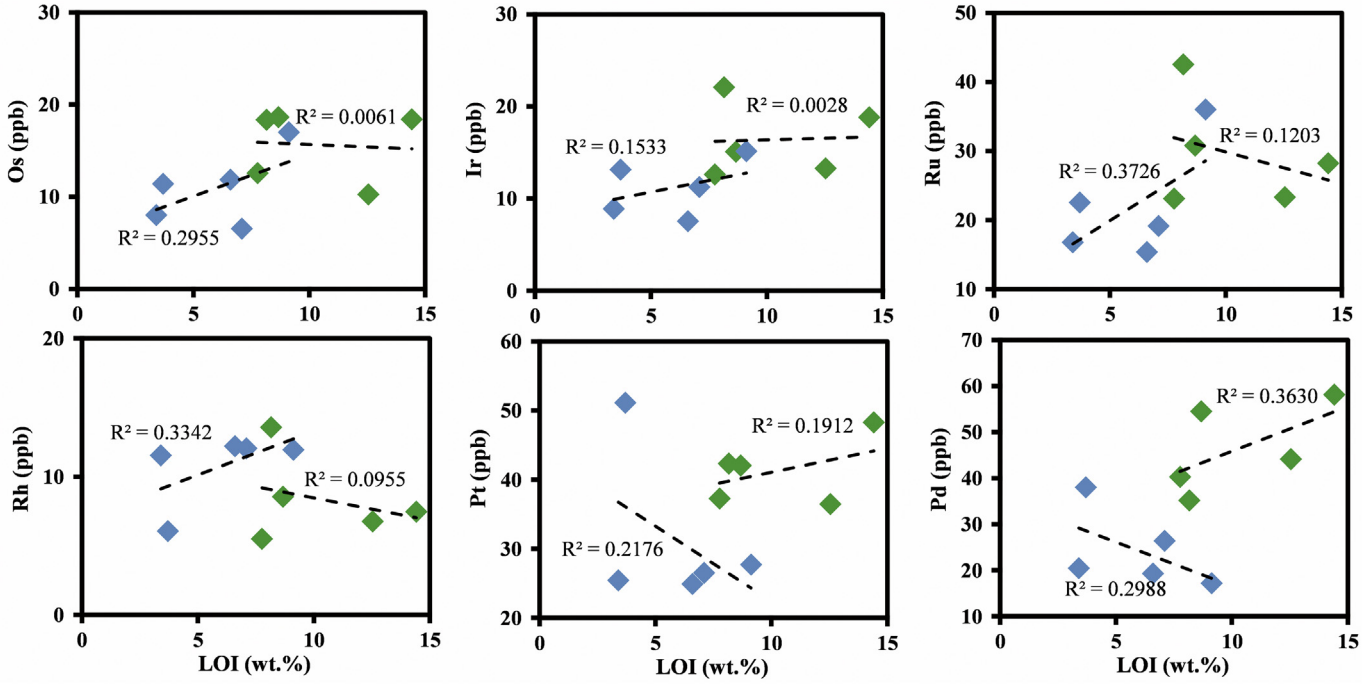

Fig. 6. Various binary plots showing loss on ignition (LOI) values against Os, Ir, Ru, Rh, Pt and Pd for the Shergol and Suru Valley ophiolitic peridotites.

Xu et al., 2020). The lower Cu/Pd ratio (i.e., 360–1939) in the studied peridotites relative to PM (ca. 7692; after McDonough and Sun, 1995) also reflects residual mantle nature (Barnes and Maier, 1999).

It has been observed that fractionation of silicates (e.g., olivines), chromites and silicate hosted sulphides (massive sulphides) control the distribution of IPGE e.g., Ir while interstitial sulphides (low melting sulphides) control the distribution of PPGE e.g., Pd (Alard et al., 2000; Naldrett, 2010; Said et al., 2011). Therefore, ratios of the Pd/Ir, Ni/Cu, Cu/Ir, Ni/Pd, Pt/Pd, Pd/Pt and Pt/Pt* can trace the effects of partial melting and crystal fractionation processes in mantle rocks (Barnes et al., 1985, 1988).

In Pd/Ir against Ni/Cu binary plot (Fig. 7a), the studied peridotites show least PGE fractionation (i.e., Pd/Ir ratio of 1.1–5.9), with higher Ni/Cu ratio (26–142) mostly lie in the mantle field following the partial melting trend of Garuti et al. (1997), and therefore, suggesting that the Pd/Ir ratio was controlled by sulphur undersaturated partial melting (Fig. 7a). Also, in Cu/Ir against Ni/Pd binary plot (Fig. 7b) of Barnes et al. (1988), the studied peridotites plot in ophiolite peridotite field and follow olivine and chromite (or Cr-spinel) fractionation trend reflecting that the PGE distribution was dominantly controlled by olivine and Cr-spinel fractionation (Naldrett, 2010; Singh et al., 2017; Saha et al., 2018). Similar observations were reported for Dazhuka ophiolitic harzburgites (Yu et al., 2001). Further, in Pt/Pt* against Pd/Ir binary plot (Fig. 7c) after Garuti et al. (1997), the studied peridotites follow partial melting trend similar to Mesozoic Neo-Tethyan ophiolite mantle peridotites (Singh et al., 2017; Saha et al., 2018) and Alpine type peridotites (Garuti et al., 1997).

Early crystallization of silicates, chromites and PGE bearing sulfides usually result in low Pt/Pd ratios while high Pd/Pt ratios (Said et al., 2011). In studied mantle peridotites, the Pt/Pd (0.8–1.6) and Pd/Pt (0.6–1.3) ratios are respectively lower and higher than PM (i.e., 1.8 and 0.5, after McDonough and Sun, 1995) reflecting early fractionation of PGE bearing silicates (e.g., olivines), chromites and sulfides. Also, the higher bulk-rock MgO contents (39.5–48.2 anhydrous wt.%), Cr, and Ni whereas, lower Pd/Ir ratios of these peridotites are consistent with higher degrees of partial melting (~18%, after Bhat et al., 2019b) but lower degrees of magmatic differentiation.

6.3. Metasomatism/melt-rock interaction

Generally, the residual mantle peridotites are characterized by flat or concave downward PGE distribution patterns (Aldanmaz and Koprubasi, 2010; Herzberg et al., 2010). Rehkamper et al. (1999), estimated 17%–25% partial melting degrees for obtaining concave downward PGE distribution patterns e.g., Ronda orogenic peridotites (Cuevas et al., 2006; Esteban et al., 2007). However, we observe concave upward PGE-distribution patterns in the studied ophiolite peridotites comparable to the various Neo-Tethyan ophiolite peridotites (Singh et al., 2013; Fig. 5). Therefore, partial melting model fails to explain the observed PGE fractionation (i.e., higher PPGE/IPGE ratios) in the studied peridotites and forces some other explanation such as, post-melting processes of fluid/melt percolation or metasomatism.

In order to evaluate the role of partial melting and/or metasomatism on PGE fractionation, Xu et al. (2020) followed the PGE modelling of Marchesi et al. (2013) and used the PGE fractionation indices such as $(Pd/Ir)_N$ and $(Pt/Ir)_N$ in combination with depletion index such as bulk-rock Al_2O_3 contents. The $(Pt/Ir)_N$ versus $(Pd/Ir)_N$ plot (Fig. 8a) shows good positive correlation whereas, $(Pd/Ir)_N$ versus Al_2O_3 (Fig. 8b) shows no correlation. In these plots, melt extraction curves were calculated using non-modal fractional melting model with a PM source containing sulphur ~300 ppm. For the calculation of fractionation curves the partition coefficient between sulphide and silicate melt for different elements are: D_{Pt}(sulfide/silicate) = 4600, D_{Pd}(sulfide/silicate) = 3500, and D_{Ir}(sulfide/silicate) = 51,000 (after Marchesi et al., 2013). The co-variation between $(Pt/Ir)_N$ and $(Pd/Ir)_N$ is attributed to similar hosts of Pt and Pd in the form of base metal sulfides in peridotites (Xu et al., 2020). Typical partial melting residues devoid of any metasomatic influence such as; orogenic massif peridotites commonly display good positive correlation among $(Pd/Ir)_N$, $(Pt/Ir)_N$ and Al_2O_3 (Bodinier and Godard, 2003). In Fig. 8, only few studied peridotite samples follow the fractional melting curves at different sulfide-silicate melt partition coefficients ($D_{sulfide/silicate}$) and most samples have higher $(Pd/Ir)_N$ for given Al_2O_3 contents (Fig. 8b). This decoupling of $(Pd/Ir)_N$ and Al_2O_3 in the studied peridotites likely reflects metasomatic processes rather than simple partial melting process at variable $D_{sulfide/silicate}$. Therefore, higher PPGE/IPGE ratios in the studied peridotites compared to typical mantle residues may be due to post-melting interaction with base metal sulfide (BMS)-rich melts (Luguet and Pearson, 2019). Thus, corroborating the above interpretation that the studied peridotites are not simple analogues of mantle peridotites.

Also, it has been suggested that the subduction-derived fluids mobilize the soluble Pd relative to insoluble Pt and adds to the mantle wedge thereby contributes higher Pd/Ir ratios (e.g., 1.1–5.9) in the studied peridotites. Therefore, such selective enrichment of highly incompatible and less refractory siderophile elements e.g., PPGE due to subduction-derived fluids to the overlying mantle wedge in a subduction setting also accounts for PGE fractionation (Xu et al., 2020). Similar results were observed in boninites of northern Tonga arc (Karrei et al., 2008) and in south Andaman ophiolite peridotites (Saha et al., 2018).

Besides, various geochemical signatures such as; highly magnesian olivines and orthopyroxenes, Cr-rich spinels (Bhat et al., 2019b), whole-rock LILE and LREE enrichments and HFSE depletions (Fig. 4a) and high Nd/Yb ratios (1.2–3) compared to low Hf/Yb ratios (0.4–1.3) demonstrate that the studied peridotites may have undergone fluid/melt metasomatism where subduction influenced melts infiltrate into the bottom of the lithosphere after earlier partial melting event (Stern, 2004; Aldanmaz et al., 2008, 2020). In subduction system, the possible end-members of the percolating melts are boninite melts and/or fore-arc basaltic melts (Dai et al., 2013; Xiong et al., 2017). The fore-arc basalts with depleted LREE signatures are analogous to NMORB (Ishizuka et al., 2018) whereas, boninite melts with enriched LILE/LREE and depleted HFSE signatures, originate by partial melting of hydrated refractory harzburgites (Woelki et al., 2018). Also, the boninite melts are usually sulphur-undersaturated as they originate from previously melted sulphur deficient mantle wedge (Zhou et al., 1998), however, the least evolved fore-arc basaltic melts are sulphur-saturated (Gannoun et al., 2016). The studied peridotites are characterized by enriched LILE/LREE ratios, depleted HFSE contents, and elevated Pd/Ir ratio with no proper sulfide phases. Therefore, boninite melts seems to be the appropriate candidate of melt metasomatism to the studied peridotites.

Further, the Cu and Pd relationship is considered as a useful indicator for the degree of sulphur-saturation of magmas (Chen and Xia, 2008). In Pd versus Cu plot (Fig. 9), the studied peridotites in comparison to Biagang peridotites from Tibet (data after Xu et al., 2020) have sulphur-undersaturated character along with boninite affinity. Therefore, we suggest that the sulphur-undersaturated boninite melts interacted with the studied peridotites.

6.4. PGE potential of western Ladakh ophiolite peridotites

Most of the world's PGE deposits are hosted in ophiolites (Ullah et al., 2020), and layered igneous intrusions e.g., Bushveld complex, where PGE mineralization occurs in differentiated basalts (Alard et al., 2000) and chromitites (Siddaiah and Masuda, 2001; Singh et al., 2013). The SSZ ophiolites are more prospective in terms of PGE-deposits as compared to mid-ocean ridge ophiolites, as the former are highly refractory (Parkinson and Pearce, 1998). The presence of sub-economic levels of noble metals (particularly PGE, Au and Ni-sulfides) in chromitites of Nidar ophiolite, eastern Ladakh (Siddaiah and Masuda, 2001) advocates potential of such metallic deposits in other ophiolites along the ISZ. The total PGE contents of various global

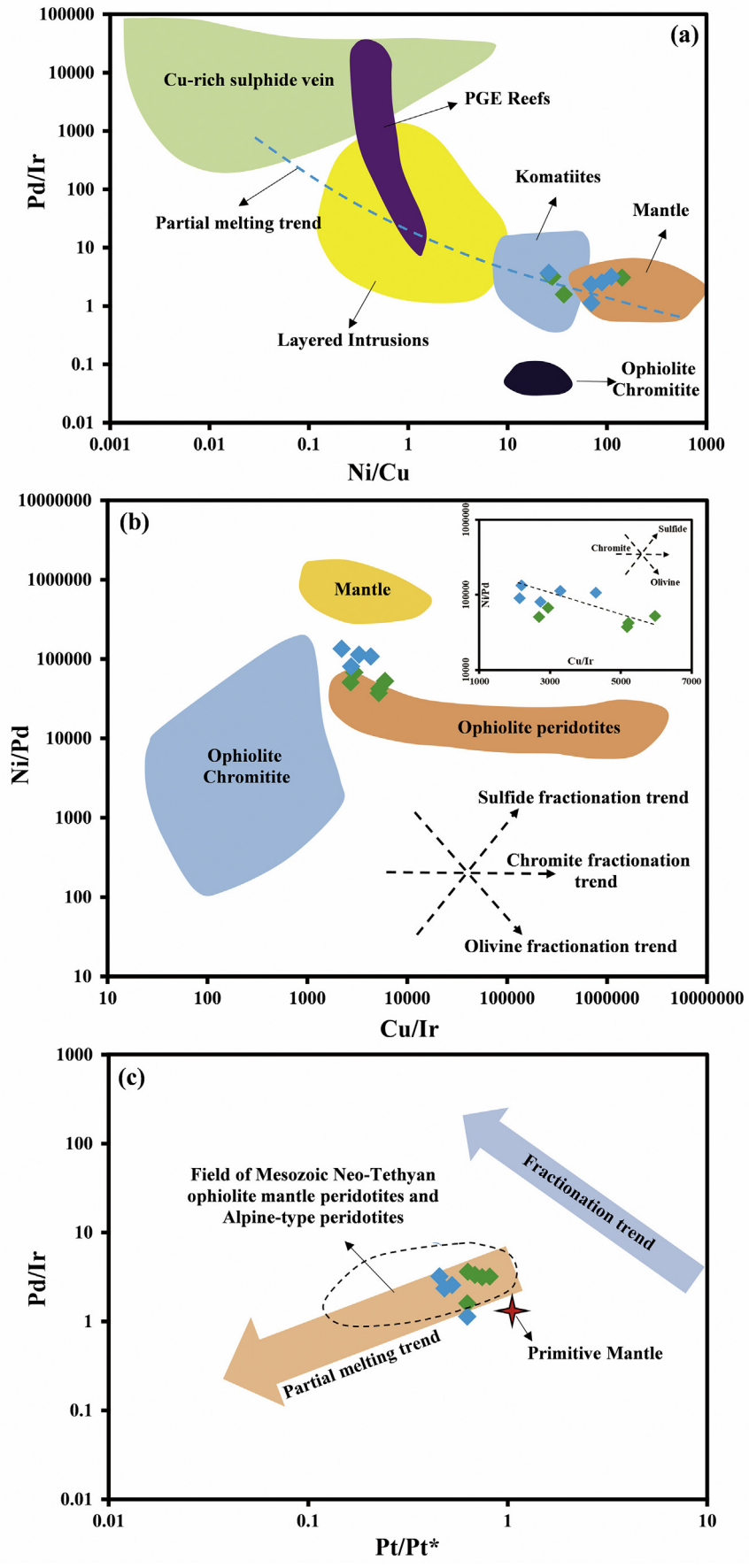

Fig. 7. Binary plots of: (a) Ni/Cu versus Pd/Ir, after Barnes (1990), (b) Cu/Ir versus Ni/Pd, after Barnes and Maier (1999), where olivine, chromite and sulphide fractionation trends are after Barnes et al. (1985), and (c) Pt/Pt* versus Pd/Ir (where fractionation and partial melting trends are from Garuti et al. (1997) and PM values after McDonough and Sun (1995)) for the Shergol and Suru Valley peridotites, western Ladakh.

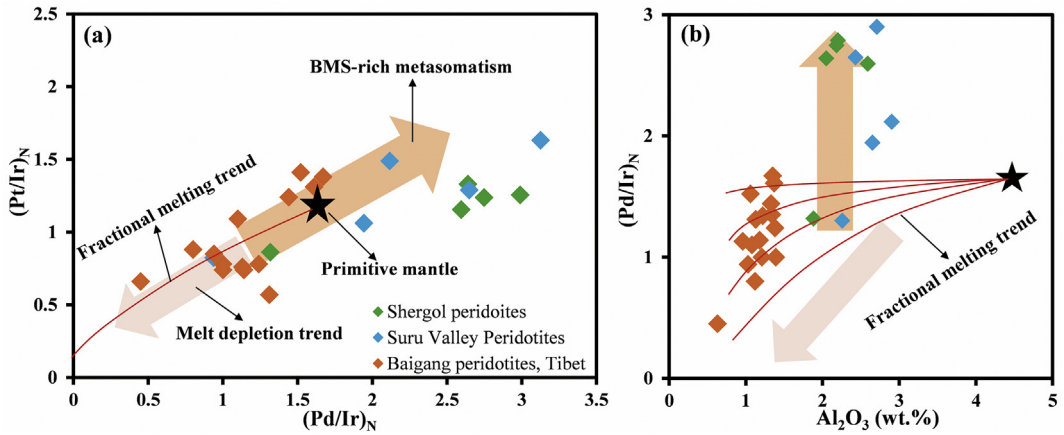

Fig. 8. (a) Whole-rock $(Pt/Ir)_N$ versus $(Pd/Ir)_N$, and (b) $(Pd/Ir)_N$ versus Al_2O_3 (anhydrous wt.%) for the Shergol and Suru Valley peridotites. Also, for comparison are shown Baigang peridotites, Tibet (after Xu et al., 2020).

ophiolitic peridotites are compiled in Table 4 with references. It is evident from the table that the total PGE contents of the studied peridotites (96–180 ppb) are much higher than that of the PM (i.e., 23.5 ppb; after McDonough and Sun, 1995) and Mesozoic Neo-Tethyan ophiolite peridotites, however, are lower than Nidar chromitites from eastern Ladakh (Fig. 5).

The PGE commonly resides in specific submicroscopic phases (less than 10 μm) in the form of platinum-group minerals (PGM) within the chromites, olivines and pyroxenes or in the interstitial silicate matrix of peridotites (Constantinides et al., 1980) and even can be accommodated in solid solution within the chromite lattice (Capobianco and Drake, 1990). However, post-magmatic alteration in the form of hydrothermal metamorphism can redistribute the PGE within the host rock, thereby giving rise to a secondary population of PGM in apparent equilibrium with low-temperature mineral assemblage i.e. ferrian-chromite, chlorite, serpentine and magnetite (Lawley et al., 2020). In the studied peridotites no good accumulation of sulfides (such as; chalcopyrite, pyrrhotite and pentlandite that commonly accompany PGE) were observed petrographically, possibly enlightening the role of sulfide liquid immiscibility. However, a good positive correlation was found in terms of the total PGE contents against Cr, Ni and MgO (Fig. 10a, b, c), reflecting possible association of PGE with chromites of the studied peridotites. Also, the studied peridotites contain anomalous Au (ranging from 40 to 91 ppb) but showing no correlation with total PGE (Fig. 10d) implying its potential hydrothermal redistribution. Even though, significant PGE, Ni, Cr and Cu enrichments were found in the Shergol and Suru Valley ophiolitic peridotites, their economic grades are not confirmed. Nevertheless, discrete sub-microscopic grains of Ni i.e., pentlandite and Cr i.e., chromite were present in these peridotites, reflecting potential for PGE enrichment elsewhere in these ophiolites, as the ophiolites are undoubtedly anomalous with respect to PGE.

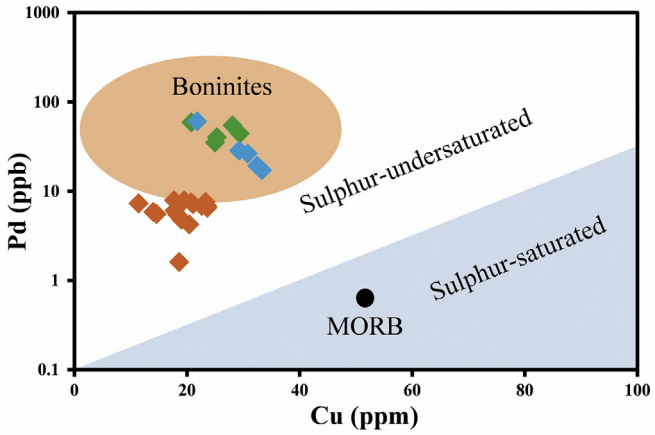

Fig. 9. Cu vs. Pd plot (after Hoatson and Keays, 1989) showing sulphur undersaturated nature of studied mantle peridotite. MORB composition after McDonough and Sun (1995).

6.5. Geochemical characteristics of mafic rocks

Based on the available age data, e.g., 140 Ma K–Ar age of Dras arc complex (Reuber et al., 1990), 140 ± 32 Ma Sm-Nd whole rock age of the Nidar ophiolitic gabbros (Ahmad et al., 2008) and 136 Ma U–Pb zircon age of Spongtang ophiolite gabbros (Buckman et al., 2018), the overall time-range of the Ladakh ophiolite mafic rocks can be bracketed between Early Cretaceous to Mid-Cretaceous. Although, the intervening period from the Cretaceous is short for radiogenic ingrowth compared to long half-life of ^{147}Sm (i.e., 1.06×10^{11} years), however, correction has been made to the measured $\varepsilon_{Nd}(t)$values. The $\varepsilon_{Nd}(t)$ values (calculated for for $t = 140$ Ma) of the Dras mafic volcanics (+5.1 to +6.6) and Shergol mafic intrusives (+5.3 to +8.6) are comparable to Spongtang ophiolitic diorites +6.6 (after Maheo et al., 2004), and Nidar ophiolitic gabbros (+6.8 to +8.8) and basic volcanics (+7.9 to +8.1) (after Ahmad et al., 2008), therefore reflecting depleted mantle source characteristics.

In order to evaluate the possibility of crustal contamination in the Shergol mafic intrusives and Dras mafic volcanics, we have plotted $^{143}Nd/^{144}Nd$ isotope ratios against differentiation indexes i.e., MgO and SiO_2 (Fig. 11). Although the studied mafic rock types display large chemical variation in terms of MgO and SiO_2 (Supplementary

Table 4
Total PGE concentration in various global ophiolitic mantle peridotites.

S. No.	Ophiolite type	∑PGE (in ppb)	Reference
1	Troodos ophiolite, Cyprus	< 20.0	Prichard and Lord (1990)
2	Dazhuka ophiolite, Tibet	< 51	Yu et al. (2001)
3	Nidar ophiolitic chromitites	< 2750	Siddaiah and Masuda (2001)
4	Manipur ophiolite complex	< 79	Singh et al. (2013)
5	Zhongba ophiolite, Tibet	< 49	Dai et al. (2011)
6	Zedang ophiolite, Tibet	< 32	Qiang et al. (2015)
7	Luobusa ophiolite peridotites	< 41	Qiang et al. (2015)
8	Nagaland-Manipur ophiolite	< 113	Singh et al. (2017)
9	Yarlung-Zangbo ophiolitic peridotites	< 40	Xu et al. (2020)

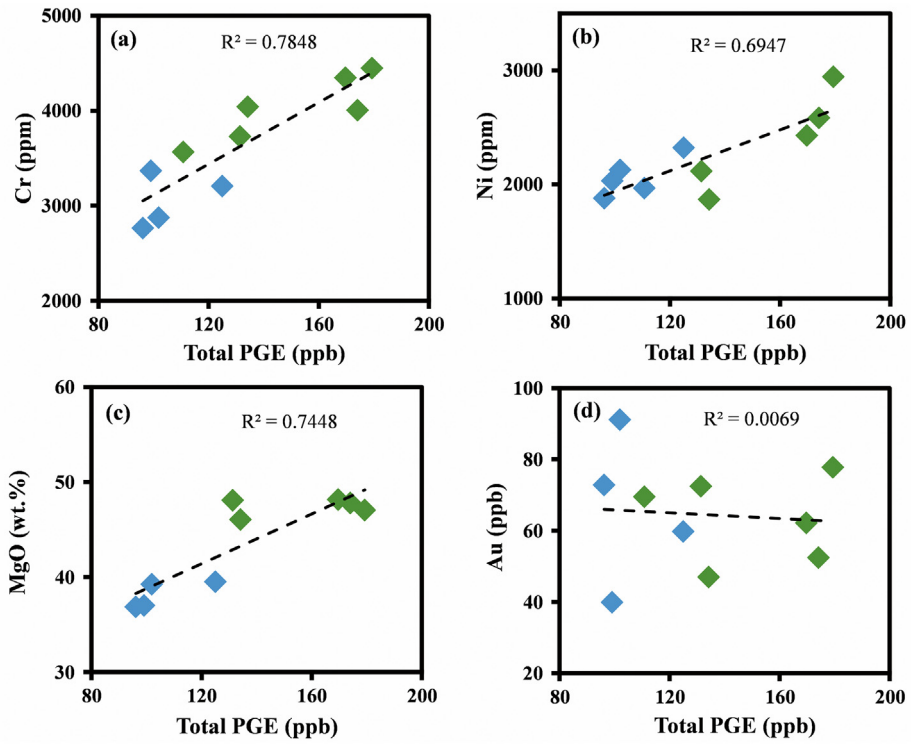

Fig. 10. Binary plots of total PGE versus (a) Cr, (b) Ni, (c) MgO, and (d) Au, for the Shergol and Suru Valley ophiolite peridotites.

Table S2), however, no correlation was observed in $\varepsilon_{Nd}(t)$ versus MgO (Fig. 11a) and $^{143}Nd/^{144}Nd$ versus SiO_2 (Fig. 11b), suggesting that there is no role of crustal contamination and the mantle source was locally homogeneous at least in terms of Nd-isotope. Also, Dras mafic volcanics and Spongtang ophiolite diorites are LREE-enriched compared to Shergol mafic intrusives and Nidar ophiolite rocks (Bhat et al., 2019c), their Nd-isotope ratios significantly overlap (Fig. 11), reflecting their derivation from similar mantle sources within an intra-oceanic arc setting far-off from any continental influence.

In subduction zones, the slab-derived components are inevitable in understanding the geochemical signature of subduction zone magmas (Saha et al., 2018). The involvement of slab-derived fluids in the studied mafic rock types is evidenced by the relative enrichment of LILE and depletion of HFSE (Fig. 4b). In addition, decoupling was observed in the studied mafic rock types in terms of $\varepsilon_{Nd}(t)$ values and LREE i.e., samples with high $\varepsilon_{Nd}(t)$ value are LREE depleted whereas, samples with low $\varepsilon_{Nd}(t)$ values are LREE enriched (Supplementary Fig. S1). This decoupling may be related to the addition of LREE-enriched fluid from a subducted slab to the mantle wedge source in an intra-oceanic arc environment. Further, in subduction zones, Th is enriched to the mantle wedge due to hydrous fluid input released from subducted slab whereas, Nb remains immobile (Zhao and Zhou, 2007; Pearce, 2008). Therefore, in the studied mafic rocks, the constant Nb/Zr ratio with increasing Th/Zr ratio (Supplementary Fig. S2) is consistent with the addition of slab-derived fluids to the mantle wedge source.

Further, the measured $\varepsilon_{Nd}(t)$ values were correlated with Tonga island arc south-west Pacific Ocean, Kohistan arc of Pakistan, Karakoram and Ladakh batholith, Nindam Formation fore-arc sediments, and Nidar ophiolite gabbros and basic volcanics (Fig. 12). From the figure, it is clear that the studied Shergol mafic intrusives and Dras mafic volcanics matches well in terms of $\varepsilon_{Nd}(t)$ range as expected with the Nidar ophiolite gabbros and basic volcanics therefore, suggesting that they are truly imbricates of a single intra-oceanic island arc in the context of Neo-Tethys Ocean.

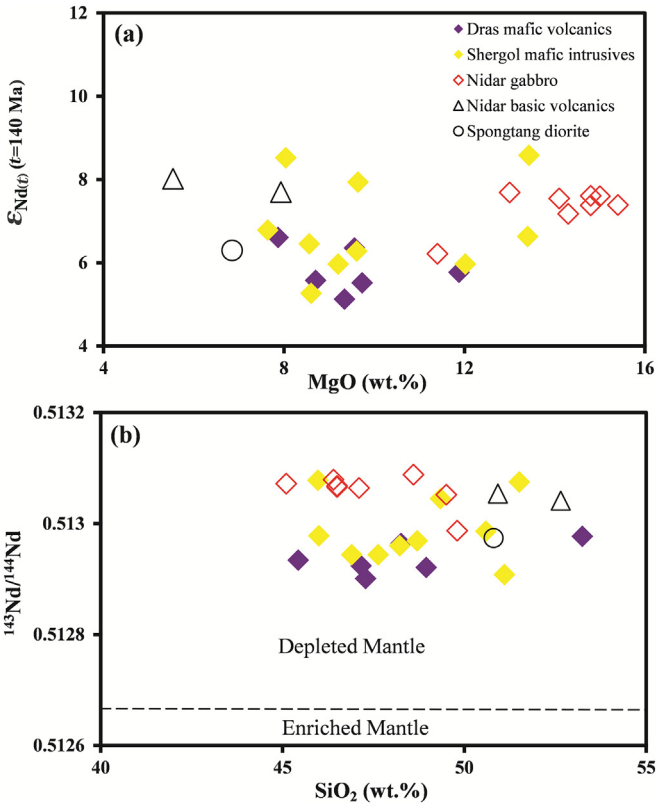

Fig. 11. Plots of: (a) MgO versus $\varepsilon_{Nd}(t)$ (t = 140 Ma), and (b) SiO_2 versus $^{143}Nd/^{144}Nd$ for the Shergol mafic intrusives and Dras mafic volcanics. Also, samples from Nidar ophiolite (data after Ahmad et al., 2008) and Spongtang ophiolite (data after Maheo et al., 2004) are shown for comparison.

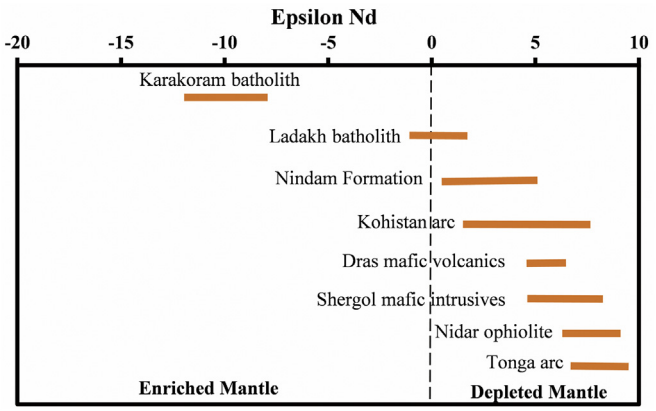

Fig. 12. Present day epsilon Nd values of the Dras mafic volcanics and Shergol mafic intrusives are compared with; Tonga arc (Ewart and Hawkesworth, 1987), Karakoram and Ladakh batholith (Allegre and Rousseau, 1988), Kohistan arc (Petterson et al., 1993), Nindam Formation (Clift et al., 2000), and Nidar ophiolite (gabbros and basic volcanics), western Ladakh (Ahmad et al., 2008).

6.6. Geodynamic framework

Based on the whole-rock geochemistry, PGE and Nd-isotope data, we suggest that the Shergol and Suru Valley ophiolitic slices evolved in an intra-oceanic arc environment in the context of the Neo-Tethys Ocean. The resulted subduction magmatism is characterized by the Shergol mafic intrusives and Dras mafic volcanics within the Neo-Tethys Ocean (Bhat et al., 2019c, and references therein). The following geodynamical model is discussed here for the origin of Shergol and Suru Valley ophiolitic slices in reference to Neo-Tethys Ocean;

The rifting of the Lhasa Terrain from the northern margin of Indian plate took place in Permo-Triassic Period thereby resulting in the opening of the Neo-Tethys Ocean (Buckman et al., 2018 and references therein; Fig. 13a). The studied Shergol and Suru Valley ophiolitic mantle peridotites preserve the signatures of depleted mantle peridotites (Bhat et al., 2019b). During Early Cretaceous (~140 Ma), there occurs an initiation of northward intra-oceanic subduction within the Neo-Tethys Ocean at the equatorial region and is reflected by the Shergol mafic intrusives intruding the Shergol and Suru Valley ophiolitic peridotites (Bhat et al., 2019b, 2019c) and Spongtang gabbros (~136 Ma) intruding the Spongtang ophiolitic peridotites (Buckman et al., 2018) thereby

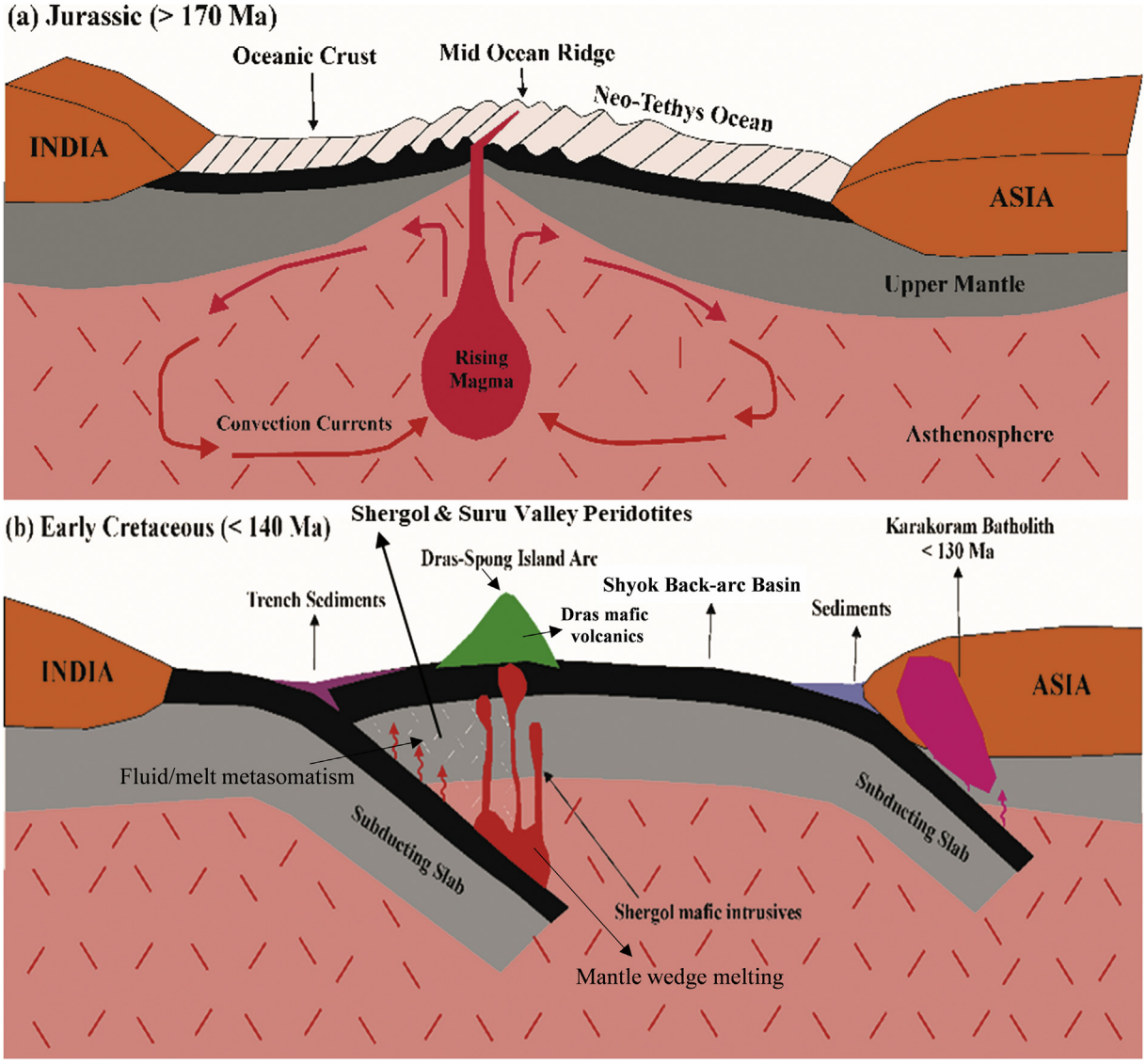

Fig. 13. Schematic diagram showing: (a) origin of the Neo-Tethys Ocean during Jurassic Period, and (b) subduction of Neo-Tethys Ocean along ISZ/Shyok Suture Zone and evolution of Shergol and Suru Valley mantle peridotites due to metasomatism thereby emplacement of Shergol mafic intrusives and Dras mafic volcanics during Early Cretaceous Period.

developing an ophiolite/arc complex. The Shergol mafic intrusives with NMORB-island arc tholeiite geochemical characteristics could be related to Spongtang ophiolite gabbros of Buckman et al. (2018), where a young and hot oceanic lithosphere undergo shallow subduction thereby causing scarce metasomatism of the overlying NMORB-type mantle wedge. With continuing subduction, the mantle wedge source became enriched in LILE thereby originating Dras mafic volcanics corresponding to Dras-Spong-Nidar island arc system during Early-Mid Cretaceous (Ahmad et al., 2008; Buckman et al., 2018) (Fig. 13b). Following this, another northward subduction initiated below the Karakoram Block (i.e., southern margin of Asia) during Early Cretaceous (~130 Ma; Heuberger et al., 2007) along the Shyok Suture Zone (Jain et al., 2012; Jagoutz et al., 2015) (Fig. 13b). During Cretaceous, both the subduction zones were magmatically active as evidenced by the geochronological data e.g., Ladakh batholith of 102 ± 2 Ma along the ISZ (Kumar et al., 2007) and Karakoram batholith of 102 ± 12 Ma to 96.7 ± 2.1 Ma (Fraser et al., 2001; Jain et al., 2012).

The transition from SSZ-type Shergol and Suru Valley peridotites to the Early Cretaceous tholeiitic Shergol mafic intrusives followed by tholeiitic to calc-alkaline Dras arc complex exhibit characteristics similar to the subduction initiation rule proposed by Whattam and Stern (2011) for Izu-Bonin-Mariana arc system. According to subduction initiation rule, the SSZ ophiolites display a series of igneous rocks that show transition from fertile mantle-derived decompression melts to increasingly metasomatized depleted mantle melts of boninite composition to typical calc-alkaline arc magmas in a manner analogous to the Tonga-Kermadec and Izu-Bonin-Marianas island arcs (Reagan et al., 2010, 2013, 2017; Whattam and Stern, 2011).

7. Conclusions

(1) The high concentration of PGE in Shergol and Suru Valley ophiolitic mantle peridotites compared to primitive mantle, most of the known global ophiolites and terrestrial magmatic reservoirs, reflect the PGE fertility of these mantle rocks.
(2) The studied peridotites follow the partial melting trend of increasing Pd/Ir with Pt/Pt*, suggesting that the PGE-distribution is controlled by partial melting process and chromite fractionation similar to Mesozoic Neo-Tethyan ophiolite mantle peridotites and Alpine type peridotites.
(3) The geochemical characteristics observed in the studied peridotites, e.g., concave upward PGE-distribution patterns, higher PPGE/IPGE ratios, enrichment in LILE and LREE can't be explained by simple partial melting model, however, the mantle wedge metasomatism – a fluid/melt interaction, is responsible for the evolution of these ophiolitic peridotites.
(4) The Shergol mafic intrusives and Dras mafic volcanics with high $^{143}Nd/^{144}Nd$ ratios and positive $\varepsilon_{Nd}(t)$ ($t = 140$ Ma) values are similar to adjoining Spongtang and Nidar ophiolitic mafic rocks and therefore may be related to the Early Cretaceous intra-oceanic island arc ophiolite system (IOIA) in the context of Neo-Tethys Ocean.
(5) Based on whole-rock, mineral and PGE geochemistry, the Shergol and Suru Valley mantle peridotites represent a portion of ancient Neo-Tethys Ocean lithospheric mantle that was subsequently trapped in a subduction zone environment, thereby evolved by an episode of metasomatism before emplacement at present positions.
(6) The transition from SSZ-type Shergol and Suru Valley ophiolitic mantle peridotites to the associated Early Cretaceous tholeiitic Shergol mafic intrusives followed by tholeiitic to calc-alkaline Dras arc complex exhibit characteristics of subduction initiation mechanism similar to the Izu-Bonin-Mariana arc system.

Supplementary data to this article can be found online at https://doi.org/10.1016/j.gsf.2020.11.014.

Declaration of Competing Interest

The authors declare that they have no known competing financial interests or personal relationships that could have appeared to influence the work reported in this paper.

Acknowledgements

The first author would like to thank Council of Scientific and Industrial Research (CSIR), New Delhi for providing financial assistance in the form of Senior Research Fellowship (CSIR-SRF). Also, thanks to Director, CSIR-National Geophysical Research Institute Hyderabad for PGE analysis. N.V. Chalapathi Rao thanks DST-SERB, New Delhi, for funding the EPMA National facility at Banaras Hindu University. The authors thank the Handling Editor Dr. Sohini Ganguly and reviewers for their insightful suggestions, which have greatly improved the quality of the manuscript.

References

Ahmad, T., Islam, R., Khanna, P.P., Thakur, V.C., 1996. Geochemistry, petrogenesis and tectonic significance of the basic volcanic units of the Zildat ophiolitic melange, Indus suture zone, eastern Ladakh (India). Geodin. Acta 9, 222–233.
Ahmad, T., Tanaka, T., Sachan, H.K., Asahara, Y., Islam, R., Khanna, P.P., 2008. Geochemical and isotopic constraints on the age and origin of the Nidar Ophiolitic complex, Ladakh, India: implications for the Neo–Tethyan subduction along the Indus suture zone. Tectonophysics 451, 206–224.
Alard, O., Griffin, W.L., Lorand, J.P., Jackson, S.E., Orielly, S.Y., 2000. Non-chondritic distribution of the highly siderophile elements in mantle sulphides. Nature 407, 891–894.
Aldanmaz, E., Koprubasi, N., 2010. Platinum-group-element systematics of peridotites from ophiolite complexes of Northwest Anatolia, Turkey: implications for mantle metasomatism by melt percolation in a supra-subduction zone environment. Int. Geol. Rev. 48, 420–442.
Aldanmaz, E., Yaliniz, M.K., Guctekin, A., Goncuoglu, M.C., 2008. Geochemical characteristics of mafic lavas from the Neotethyan ophiolites in western Turkey: implications for heterogeneous source contribution during variable stages of ocean crust generation. Geol. Mag. 145, 37–54.
Aldanmaz, E., van Hinsbergen, D.J., Yildiz-Yuksekol, O., Schmidt, M.W., McPhee, P.J., Meisel, T., Guctekin, A., Mason, P.R., 2020. Effects of reactive dissolution of orthopyroxene in producing incompatible element depleted melts and refractory mantle residues during early fore-arc spreading: Constraints from ophiolites in eastern Mediterranean. Lithos 360.
Allegre, C.J., Rousseau, D., 1988. Nd-Sr isotopic study of Himalaya Tibet gneiss and granitoids. Development of the Asian continental crust since Jurassic time. Chem. Geol. 70, 66.
Ao, A., Bhowmik, S.K., Upadhyay, D., 2020. PT-melt/fluid evolution of abyssal mantle peridotites from the Nagaland Ophiolite complex, NE India: Geodynamic significance. Lithos 354, 105344.
Arai, S., Miura, M., 2016. Formation and modification of chromitites in the mantle. Lithos 264, 277–295.
Arai, S., Kadoshima, K., Morishita, T., 2006. Widespread arc-related melting in the mantle section of the northern Oman ophiolite as inferred from detrital chromian spinels. J. Geol. Soc. Lond. 163, 869–879.
Balaram, V., 2008. Recent advances in the determination of PGE in exploration studies – a review. J. Geol. Soc. India 72, 661–677.
Barnes, S.J., 1990. The use of metal ratios in prospecting for a platinum group element deposit. J. Explor. Geochem. 37, 91–99.
Barnes, S.J., Maier, W.D., 1999. The fractionation of Ni, Cu and the noble metals in silicate and sulfide liquids. In: Keays, R.R., Lesher, C.M., Lightfoot, P.C., Farrow, C.E. (Eds.), Dynamic Processes in Magmatic Ore Deposits and Their Application in Mineral Exploration, Geological Association of Canada Short Course Notes, pp. 69–106.
Barnes, S.J., Naldrett, A.J., Gorton, M.P., 1985. The origin of the fractionation of platinum-group elements in terrestrial magmas. Chem. Geol. 53, 303–323.
Barnes, S.J., Boyd, R., Korneliussen, A., Nilsson, L.P., Often, M., Pedersen, R.B., Robins, B., 1988. The use of mantle normalization and metal ratios in discriminating between the effects of partial melting, crystal fractionation and sulphide segregation on platinum group elements, gold, nickel, and copper: Examples from Norway. In: Prichard, H.M., Potts, P.J., Bowles, S.J., Cripp, S.J. (Eds.), Geoplatinum. Elsevier, London, pp. 113–143.
Barth, M.G., Mason, P.R.D., Davies, G.R., Drury, M.R., 2008. The Othris Ophiolite, Greece: a snapshot of subduction initiation at a mid-ocean ridge. Lithos 100, 234–254.
Bhat, I.M., Ahmad, T., Subba Rao, D.V., 2017. Geochemical characterization of serpentinized peridotites from the Shergol ophiolitic slice along the Indus Suture Zone (ISZ), Ladakh Himalaya, India. J. Geol. 125, 501–513.
Bhat, I.M., Ahmad, T., Subba Rao, D.V., 2019a. The tectonic evolution of Dras arc complex along Indus Suture Zone, western Himalaya: Implications for Neo–Tethys geodynamics. J. Geodyn. 124, 52–66.
Bhat, I.M., Ahmad, T., Subba Rao, D.V., 2019b. Origin and evolution of Suru Valley ophiolite peridotite slice along Indus suture zone, Ladakh Himalaya, India: Implications on

melt–rock interaction in a subduction zone environment. Chemie der Erde Geochem. 79, 78–93.
Bhat, I.M., Ahmad, T., Subba Rao, D.V., 2019c. Petrology and geochemistry of mafic intrusive rocks from the Sapi–Shergol ophiolitic mélange, Indus Suture Zone, western Ladakh: Constraints on petrogenesis and tectonic setting. J. Geol. 127, 543–566.
Bodinier, J.L., Godard, M., 2003. Orogenic, ophiolitic and abyssal peridotites. In: Carlson, R.W. (Ed.), Treatise on Geochemistry. The Mantle and Core vol. 2. Elsevier, Amsterdam, pp. 103–170.
Brookfield, M.E., Reynolds, P.H., 1981. Late Cretaceous emplacement of the Indus suture zone ophiolitic melanges and an Eocene–Oligocene magmatic arc on the northern edge of the Indian plate. Earth Planet. Sci. Lett. 55, 157–162.
Brugmann, G.E., Naldrett, A.J., Asif, M., Lightfoot, P.C., Gorbachev, N.S., Fedorenko, V.A., 1993. Siderophile and chalcophile metals as tracers of the evolution of the Siberian Trap in the Noril'sk region, Russia. Geochim. Cosmochim. Acta 57, 2001–2018.
Buckman, S., Aitchison, J.C., Nutman, A., Bennett, V., Saktura, W.M., Walsh, J., Kachovich, S., Hidaka, H., 2018. The Spongtang Massif in Ladakh, NW Himalaya: an early cretaceous record of spontaneous, intra–oceanic subduction initiation in the Neotethys. Gondwana Res. 63, 226–249.
Canil, D., 2004. Mildly incompatible elements in peridotites and the origins of mantle lithosphere. Lithos 77, 375–393.
Capobianco, C.J., Drake, M.J., 1990. Partitioning of ruthenium, rhodium, and palladium between spinel and silicate melt and implications for platinum group element fractionation trends. Geochim. Cosmochim. Acta 54, 869–874.
Chatterjee, S., Goswami, A., Scotese, C.R., 2013. The longest voyage: tectonic, magmatic, and paleoclimatic evolution of the Indian plate during its northward flight from Gondwana to Asia. Gondwana Res. 23, 238–267.
Chen, G.W., Xia, B., 2008. Platinum group elemental geochemistry of Mafic and Ultramafic rocks from the Xigaze Ophiolite, Southern Tibet. J. Asian Earth Sci. 32, 406–422.
Clift, P.D., Degnan, P.J., Hannigan, R., Blusztajn, J., 2000. Sedimentary and geochemical evolution of the Dras fore-arc basin, Indus Suture, Ladakh Himalaya, India. Geol. Soc. Am. Bull. 112, 450–466.
Clift, P.D., Hannigan, R., Blusztajn, J., Draut, A.E., 2002. Geochemical evolution of the Dras–Kohistan Arc during collision with Eurasia: evidence from the Ladakh Himalaya, India. Island Arc 11, 255–273.
Coleman, R.G., 1977. Ophiolites–Ancient Continental Lithosphere. Springer–Verlag, NewYork, Berlin, p. 220.
Constantinides, C.C., Kingston, G.A., Fisher, P.C., 1980. The occurrence of platinum group minerals in the chromitites of the Kokkinorotsos chrome mine, Cyprus. In: Panayiotou, A. (Ed.), Ophiolites, Proceedings of the International Ophiolite Symposium. Cyprus. Geological Survey Department, Nicosia Cyprus, pp. 93–101.
Corfield, R.I., Searle, M.P., Pedersen, R.B., 2001. Tectonic setting, origin, and obduction history of the Spontang ophiolite, Ladakh Himalaya, NW India. J. Geol. 109, 715–736.
Crocket, J.H., Paul, D.K., Trisha, L., 2013. Platinum-group elements in the Eastern Deccan volcanic province and a comparison with platinum metals of the western Deccan. J. Earth Syst. Sci. 122, 1035–1044.
Cuevas, J., Esteban, J.J., Tubía, J.M., 2006. Tectonic implications of the granite dyke swarm in the Ronda peridotites (Betic Cordilleras, Southern Spain). J. Geol. Soc. Lond. 163, 631–640.
Dai, J., Wang, C., Hebert, R., Santosh, M., Li, Y., Xu, J., 2011. Petrology and geochemistry of peridotites in the Zhongba ophiolite, Yarlung Zangbo Suture Zone: implications for the early cretaceous intraoceanic subduction zone within the Neo-Tethys. Chem. Geol. 288, 133–148.
Dai, J., Wang, C., Polat, A., Santosh, M., Li, Y., Ge, Y., 2013. Rapid forearc spreading between 130 and 120 Ma: evidence from geochronology and geochemistry of the Xigaze ophiolite, southern Tibet. Lithos 172, 1–16.
Deschamps, F., Guillot, S., Godard, M., Chauvel, C., Andreani, M., Hattori, K., 2010. In situ characterization of serpentinites from forearc mantle wedges: timing of serpentinization and behavior of fluid–mobile elements in subduction zones. Chem. Geol. 269, 262–277.
Deschamps, F., Godar, M., Guillot, S., Hattori, K., 2013. Geochemistry of subduction zone serpentinites: a review. Lithos 178, 96–127.
Dilek, Y., Furnes, H., 2009. Structure and geochemistry of Tethyan ophiolites and their petrogenesis in subduction rollback systems. Lithos 113, 1–20.
Dilek, Y., Furnes, H., 2011. Ophiolite genesis and global tectonics: geochemical and tectonic fingerprinting of ancient oceanic lithosphere. Geol. Soc. Am. Bull. 123, 387–411.
Esteban, J.J., Cuevas, J., Tubía, J.M., Liati, A., Seward, D., Gebauer, D., 2007. Timing and origin of zircon-bearing chlorite schists in the Ronda peridotites (Betic Cordilleras, Southern Spain). Lithos 99, 121–135.
Ewart, A., Hawkesworth, C.J., 1987. The Pleistocene–recent Tonga–Kermadec arc lavas: Interpretation of new isotopic and rare earth data in terms of a depleted source mantle. J. Petrol. 28, 495–530.
Frank, W., Gansser, A., Trommsdorff, V., 1977. Geological observations in the Ladakh area (Himalayas)–a preliminary report. Schweiz. Mineral. Petrogr. Mitt. 57, 89–113.
Fraser, J., Searle, M.P., Parrish, R., Noble, S., 2001. Chronology of deformation, metamorphism, and magmatism in the southern Karakoram Mountains. Geol. Soc. Am. Bull. 113, 1443–1455.
Fu, C., Yan, Z., Aitchison, J.C., Guo, X., Xia, W., 2019. Abyssal and Suprasubduction Peridotites in the Lajishan Ophiolite Belt: Implication for initial Subduction of the Proto-Tethyan Ocean. J. Geol. 127, 398–410. https://doi.org/10.1086/703488.
Gammons, C.H., Bloom, M.S., Yu, Y., 1992. Experimental investigation of the hydrothermal geochemistry of platinum and palladium: I. Solubility of platinum and palladium sulfide minerals in NaCl/H_2SO_4 solutions at 300 °C. Geochim. Cosmochim. Acta 56, 3881–3894.
Gannoun, A., Burton, K.W., Day, J.M.D., Harvey, J., Schiano, P., Parkinson, I., 2016. Highly siderophile element and Os isotope systematics of volcanic rocks at divergent and convergent plate boundaries and in intraplate settings. Rev. Mineral. Geochem. 81, 651–724.
Gansser, A., 1964. The Geology of the Himalayas. 289. Wiley Interscience, New York.
Gansser, A., 1980. The significance of the Himalaya suture zone. Tectonophysics 62, 37–40.
Garuti, G., Fershtater, G., Bea, F., Montero, P., Pushkarev, E.V., Zaccarini, F., 1997. Platinum-group elements as petrological indicators in mafic-ultramafic complexes of the central and southern Urals: preliminary results. Tectonophysics 276, 181–194.
Ghosh, B., Bandyopadhyay, D., Morishita, T., 2017. Andaman-Nicobar ophiolites, India: origin, evolution and emplacement. Geol. Soc. Lond. Mem. 47, 95–110.
Goldfarb, R., Baker, T., Dube, B., Groves, D.I., Hart, C.J., Gosselin, P., 2005. Distribution, character and genesis of gold deposits in metamorphic terranes. In: Hedenquist, J.W., Thompson, J.F.H., Goldfarb, R.G., Richards, J.P. (Eds.), Economic Eeology 100th Anniversary Volume. Society of Economic Geologists, Littleton, Colorado, USA, pp. 407–450.
Hanley, J.J., Mungall, J.E., Pettke, T., Spooner, E.T.C., Bray, C.J., 2008. Fluid and halide melt inclusions of magmatic origin in the ultramafic and lower banded series, Stillwater complex, Montana, USA. J. Petrol. 49, 1133–1160.
Herzberg, C., Condie, K., Korenaga, J., 2010. Thermal history of the Earth and its petrological expression. Earth Planet. Sci. Lett. 292, 79–88.
Heuberger, S., Schaltegger, U., Burg, J.P., Villa, I.M., Frank, M., Dawood, H., Zanchi, A., 2007. Age and isotopic constraints on magmatism along the Karakoram-Kohistan Suture Zone, NW Pakistan: evidence for subduction and continued convergence after India-Asia collision. Swiss J. Geosci. 100, 85–107.
Hoatson, D.M., Keays, R.R., 1989. Formation of platiniferous sulide horizons by crustal fractionation and magma mixing in the Munni Munni layered intrusion, West Pilbara Block, West Australia. Econ. Geol. 84, 1775–1804.
Honegger, K., Dietrich, V., Frank, W., Gansser, A., Thoni, M., Trommsdorf, V., 1982. Magmatic and metamorphism in the Ladakh Himalayas (the Indus–Tsangpo suture zone). Earth Planet. Sci. Lett. 60, 253–292.
Ishikawa, A., Kaneko, Y., Kadarusman, A., Ota, T., 2007. Multiple generations of forearcmaficeultramafic rocks in the TimoreTanimbar ophiolite, eastern Indonesia. Gondwana Res. 11, 200–217.
Ishizuka, O., Hickey Vargas, R., Arculus, R.J., Yogodzinski, G.M., Savov, I.P., Kusano, Y., McCarthy, A., Brandl, P.A., Sudo, M., 2018. Age of Izu–Bonin–Mariana arc basement. Earth Planet. Sci. Lett. 481, 80–90.
Jagoutz, O., Royden, L., Holt, A.F., Becker, T.W., 2015. Anomalously fast convergence of India and Eurasia caused by double subduction. Nat. Geosci. 8, 475–478.
Jain, A.K., Ahmad, T., Singh, S., Ghosh, S.K., Patel, R.C., Kumar, R., Bhargava, O.N., 2012. Evolution of the Himalaya. Proceedings of the Indian Natural Science Academy. 78, pp. 259–275.
Karrei, L.I., Mungall, J.E., Jenner, F., Arculus, R.J., Mavrogenes, J.A., 2008. Elevated Pt, Pd and au concentrations in high-Ca boninites, northern Tonga arc: evidence for residual monosulphide solid solution. Geophys. Res. Abstr. 10 (EGU 2008-A-04326).
Kelemen, P.B., Dick, H.J.B., Quick, J.E., 1992. Formation of harzburgite by pervasive melt/rock reaction in the upper mantle. Nature 358, 635–641.
Kepezhinskas, P., Defant, M.J., Widom, E., 2002. Abundance and distribution of PGE and au in the island-arc mantle: implications for sub-arc metasomatism. Lithos 60, 113–128.
Khogenkumar, S., Singh, A.K., Bikramaditya Singh, R.K., Khanna, P.P., Singh, N.I., Singh, W.I., 2016. Coexistence of MORB and OIB-type mafic volcanics in the Manipur Ophiolite complex, Indo-Myanmar Orogenic Belt, Northeast India: implication for heterogeneous mantle source at the spreading zone. J. Asian Earth Sci. 116, 42–58.
Kingson, O., Bhutani, R., Dash, J.K., Sebastian, S., Balakrishnan, S., 2017. Resolving the conundrum in origin of the Manipur Ophiolite complex, Indo-Myanmar range: Constraints from Nd isotopic ratios and elemental concentrations in serpentinized peridotite. Chem. Geol. 460, 117–129.
Kumar, R.N., Lal, N., Singh, S., Jain, A.K., 2007. Cooling and exhumation of the Trans-Himalayan Ladakh batholith as constrained by fission track apatite and zircon ages. Curr. Sci. 90, 490–496.
Lawley, C.J.M., Petts, D.C., Jackson, S.E., Zagorevski, A., Pearson, D.G., Kjarsgaard, B.A., Savard, D., Tschirhart, V., 2020. Precious metal mobility during serpentinization and destabilization of base metal sulphide. Lithos 354, 105278. https://doi.org/10.1016/j.105278.
Leat, P.T., Pearce, J.A., Barker, P.F., Millar, I.L., Barry, T.L., Larter, R.D., 2004. Magma genesis and mantle flow at a subducting slab edge: the South Sandwich arc–basin system. Earth Planet. Sci. Lett. 227, 17–35.
Lorand, J.P., Keays, R.R., Bodinier, J.L., 1993. Copper and noble metal enrichments across the lithosphere-asthenosphere boundary of mantle diapirs: evidence from the Lanzo lherzolite massif. J. Petrol. 34, 1110–1140.
Lorand, J.P., Reisberg, L., Bedini, R.M., 2003. Platinum-group elements and melt percolation processes in Sidamo spinel peridotite xenoliths, Ethiopia, East African Rift. Chem. Geol. 196, 57–75.
Lorand, J.P., Luguet, A., Alard, O., 2008. Platinum-group elements: a new set of key tracers for the Earth's interior. Elements 4, 247–252.
Luguet, A., Pearson, G., 2019. Dating mantle peridotites using Re-Os isotopes: the complex message from whole rocks, base metal sulfides, and platinum group minerals. Am. Mineral. 104, 165–189.
Maheo, G., Bertrand, H., Guillot, S., Villa, I.M., Keller, F., Capiez, P., 2004. The South Ladakh ophiolites (NW Himalaya, India): an intraoceanic tholeiitic origin with implication for the closure of the Neo-Tethys. Chem. Geol. 203, 273–303.
Manikyamba, C., Saha, A., 2014. PGE geochemistry of komatiites from Neoarchean Sigegudda greenstone terrane, western Dharwar Craton, India. Proceedings of the Workshop on Magmatic Ore Deposits. 2. J. Geol. Soc. India, Special Publication, pp. 162–174.
Marchesi, C., Garrido, C.J., Harvey, J., Gonzalez-Jimenez, J.M., Hidas, K., Lorand, J.P., Gervilla, F., 2013. Platinum-group elements, S, Se and Cu in highly depleted abyssal peridotites

from the Mid-Atlantic Ocean Ridge (ODP Hole 1274A): influence of hydrothermal and magmatic processes. Contrib. Mineral. Petrol. 166, 1521–1538.
McDonough, W.F., Sun, S.S., 1995. The composition of the Earth. Chem. Geol. 120, 223–253.
Moghadam, H.S., Corfu, F., Chiaradia, M., Stern, R.J., Ghorbani, G., 2014. Sabzevar Ophiolite, NE Iran: progress from embryonic oceanic lithosphere into magmatic arc constrained by new isotopic and geochemical data. Lithos 210, 224–241.
Molnar, P., Tapponnier, P., 1975. Cenozoic tectonics of Asia; effects of a continental collision. Science 189, 419–426.
Mondala, S.K., Khatunb, S., Prichardc, H.M., Satyanarayanan, M., Kumar, G.R.V., 2019. Platinum-group element geochemistry of boninite-derived Mesoarchean chromitites and ultramafic-mafic cumulate rocks from the Sukinda Massif (Orissa, India). Ore Geol. Rev. 104, 722–744.
Moores, E.M., Kellogg, L., Dilek, Y., 2000. Tethyan ophiolites and mantle convection and tectonic historical contingency: A resolution of the ophiolite conundrum. In: Dilek, Y., Moores, E.M., Elthon, D., Nicolas, A. (Eds.), Ophiolite and Oceanic Crust: New Insights from Field Studies and Ocean Drilling Program. Geological Society of America Special Paper vol. 349, pp. 3–12.
Naldrett, A.J., 2010. Secular variation of magmatic sulfide deposits and their source magmas. Econ. Geol. 105, 669–688.
Naldrett, A.J., Duke, J.M., 1980. Platinum metals in magmatic sulfide ores. Science 208, 1417–1424.
Niu, Y., 2004. Bulk–rock Major and trace element compositions of abyssal peridotites: implications for mantle melting, melt extraction and post–melting processes beneath mid-ocean ridges. J. Petrol. 45, 2423–2458.
Pal, T., Bhattacharya, A., Nagendran, G., Yanthan, N.M., Singh, R., Raghumani, N., 2014. Petrogenesis of chromites from the Manipur ophiolite belt, NE India: evidence for a supra-subduction zone setting prior to Indo-Myanmar collision. Mineral. Petrol. 108, 713–726.
Pan, P., Wood, S.A., 1994. Solubility of Pt and Pd sulfides and Au metal in aqueous bisulfide solutions. Mineral. Deposita 29, 373–390.
Parkinson, I.J., Pearce, J.A., 1998. Peridotites from the Izu-Bonin-Mariana forearc (ODP Leg 125): evidence for mantle melting and melt-mantle interaction in a supra subduction zone setting. J. Petrol. 39, 1577–1618.
Parlak, O., Bagci, U., Rizaoglu, T., Ionescu, C., Onal, G., Hock, V., Kozlu, H., 2020. Petrology of ultramafic to mafic cumulate rocks from the Goksun (Kahramanmaraş) ophiolite, Southeast Turkey. Geosci. Front. 11, 109–128.
Pearce, J.A., 2003. Supra-Subduction Zone Ophiolites: the Search for Modern Analogues. Special Papers-Geological Society of America, pp. 269–294.
Pearce, J.A., 2008. Geochemical fingerprinting of oceanic basalts with applications to ophiolite classification and the search for Archean oceanic crust. Lithos 100, 14–48.
Pedersen, R.B., Searle, M.P., Corfield, R.I., 2001. U–Pb zircon ages from the Spontang Ophiolite, Ladakh Himalaya. J. Geol. Soc. Lond. 158, 513–520.
Petterson, M.G., Crawford, M.B., Windley, B.F., 1993. Petrogenetic implications of neodymium isotope data from the Kohistan Batholith, North Pakistan. J. Geol. Soc. Lond. 150, 125–129.
Piccardo, G.B., Zanetti, A., Muntener, O., 2007. Melt/peridotite interaction in the Southern Lanzo peridotite: field, textural and geochemical evidence. Lithos 94, 181–209.
Prichard, H.M., Lord, R.A., 1990. Platinum and palladium in the Troodos ophiolite complex. Cyprus. Canadian Mineralogist 28 (3), 607–617.
Qian, Q., Hermann, J., Donga, F., Lina, L., Sun, B., 2020. Episodic formation of Neotethyan ophiolites (Tibetan plateau): Snapshots of abrupt global plate reorganizations during major episodes of supercontinent breakup? Earth-Sci. Rev. https://doi.org/10.1016/j.earscirev.2020.103144.
Qiang, L., Bin, X., Jianfeng, L., Lianze, X., Qiangtai, H., Zhongyu, X., 2015. Mineral chemistry and geochemistry of peridotites from theZedang and Luobusa Ophiolites, Tibet: Implications for theEvolution of the Neo-Tethys. J. Earth Sci. 26, 893–910.
Radhakrishna, T., Divakara Rao, V., Murali, A.V., 1987. Geochemistry and petrogenesis of ultramafic and mafic plutonic rocks of the Dras ophiolitic mélange, Indus suture (northwest Himalaya). Earth Planet. Sci. Lett. 82, 136–144.
Radhakrishna, T., Divakara Rao, V., Murali, A.V., 1984. Geochemistry of Dras volcanics and the evolution of the Indus suture ophiolites. Tectonophysics 108, 135–153.
Reagan, M.K., Ishizuka, O., Stern, R.J., Kelley, K.A., Ohara, Y., Blichert-Toft, J., Bloomer, S.H., Cash, J., Fryer, P., Hanan, B., Hickey-Vargas, R., Ishii, T., Kimura, J.I., Peate, D.W., Rowe, M.C., Woods, M., 2010. Fore-arc basalts and subduction initiation in the Izu-Bonin-Mariana system. Geochem. Geophys. Geosyst. 11, 1–17.
Reagan, M.K., McClelland, W.C., Girard, G., Goff, K.R., Peate, D.W., Ohara, Y., Stern, R.J., 2013. The geology of the southern Mariana fore–arc crust: Implications for the scale of Eocene volcanism in the western Pacific. Earth Planet. Sci. Lett. 380, 41–51.
Reagan, M.K., Pearce, J.A., Petronotis, K., Almeev, R.R., Avery, A.J., Carvallo, C., Chapman, T., Christeson, G.L., Ferre, E.C., Godard, M., Heaton, D.E., Kirchenbaur, M., Kurz, W., Kutterolf, S., Li, H., Li, Y., Michibayashi, K., Morgan, S., Nelson, W.R., Prytulak, J., Python, M., Robertson, A.H.F., Ryan, J.G., Sager, W.W., Sakuyama, T., Shervais, J.W., Shimizu, K., Whattam, S.A., 2017. Subduction initiation and ophiolite crust: New insights from IODP drilling. Int. Geol. Rev. 59, 1439–1450.
Rehkamper, M., Halliday, A.N., Fitton, J.G., Lee, D.C., Wieneke, M., Arndt, N.T., 1999. Ir, Ru, Pt and Pd in basalts and komatiites: new constraints for the geochemical behaviour of the platinum-group elements in the mantle. Geochim. Cosmochim. Acta 63, 3915–3934.
Reuber, I., 1989. The Dras Arc - two successive volcanic events on eroded oceanic–crust. Tectonophysics 161, 93–106.
Reuber, I., Montigny, R., Thuizat, R., Heitz, A., 1990. K/Ar ages of ophiolites and arc volcanics of the Indus suture zone (Ladakh): comparison with other Himalaya – Karakorum data. J. Himal. Geol. 1, 115–125.
Robertson, A.H.F., 2000. Formation of melanges in the Indus suture zone, Ladakh Himalaya by successive subduction-related, collisional and post-collisional processes during late Mesozoic late tertiary time. In: Khan, M.A., Treloar, P.J., Searle, M.P., Khan, M.Q. (Eds.), Tectonics of the Nanga Parbat Syntaxis and the Western Himalaya. Geological Society of London, Special Publication vol. 170, pp. 333–374.
Rollinson, H., 1993. Using Geochemical Data: Evaluation, Presentation, Pnterpretation. Longman-Wyllie, Harlow/New York, p. 352.
Rollinson, H., Adetunji, J., 2013. Mantle podiform chromitites do not form beneath mid-ocean ridges: a case study from the Moho transition zone of the Oman ophiolite. Lithos 177, 314–327.
Saccani, E., 2015. A new method of discriminating different types of post Archean ophiolitic basalts and their tectonic significance using Th-Nb and Ce-Dy-Yb systematics. Geosci. Front. 6, 481–501.
Saha, A., Dhang, A., Ray, J., Chakraborty, S., Moecher, D., 2010. Complete preservation of ophiolite suite from south Andaman, India: a mineral-chemical perspective. J. Earth Syst. Sci. 119, 365–381.
Saha, A., Manikyamba, C., Santosh, M., Ganguly, S., Khelen, A.C., Subramanyam, K.S.V., 2015. Platinum Group elements (PGE) geochemistry of komatiites and boninites from Dharwar Craton, India: implications for mantle melting processes. J. Asian Earth Sci. 105, 300–319.
Saha, A., Santosh, M., Ganguly, S., Manikyamba, C., Ray, J., Dutta, J., 2018. Geochemical cycling during subduction initiation: evidence from serpentinized mantle wedge peridotite in the south Andaman ophiolite suite. Geosci. Front. 9, 1755–1775.
Said, N., Kerrich, R., Maier, W.D., McCuaig, C., 2011. Behaviour of Ni–PGE–Au–Cu in mafic–ultramafic volcanic suites of the 2.7 Ga Kambalda Sequence, Kalgoorlie Terrane, Yilgarn Craton. Geochim. Cosmochim. Acta 75, 2882–2910.
Searle, M.P., Windley, B.F., Coward, M.P., Cooper, D.J.W., Rex, A.J., Rex, D., Tingdong, L., Xuchang, X., Jan, M.Q., Thakur, V.C., Kumar, S., 1987. The closing of Tethys andthe tectonics of the Himalaya. Geol. Soc. Am. Bull. 98, 678–701.
Shervais, J.W., 2001. Birth, death, and resurrection: the life cycle of suprasubduction zone ophiolites. Geochem. Geophys. Geosyst. 2 (2000GC000080).
Siddaiah, N.S., Masuda, A., 2001. Noble metals in the Nidar ophiolite of the Indus Suture Zone, eastern Ladakh, Himalaya, India. Geol. Surv. India Spec. Publ. 58, 465–469.
Singh, A.K., Debala Devi, L., Ibotombi Singh, N., Subramanyam, K.S.V., Bikramaditya Singh, R.K., Satyanarayanan, M., 2013. Platinum-group elements and gold distributions in peridotites and associated podiform chromitites of the Manipur Ophiolitic complex, Indo-Myanmar Orogenic Belt, Northeast India. Chemie der Erde Geochem. 73, 147–161.
Singh, M.R., Manikyamba, C., Ray, J., Ganguly, S., Santosh, M., Saha, A., Rambabu, S., Sawant, S.S., 2016. Major, trace and platinum group element (PGE) geochemistry of Archean Iron Ore Group and Proterozoic Malangtoli metavolcanic rocks of Singhbhum Craton, Eastern India: inferences on mantle melting and Sulphur saturation history. Ore Geol. Rev. 72, 1263–1289.
Singh, A.K., Nayak, R., Khogenkumar, S., Subramanyam, K.S.V., Thakur, S.S., Bikramaditya Singh, R.K., Satyanarayanan, M., 2017. Genesis and tectonic implications of cumulate pyroxenites and tectonite peridotites from the Nagaland–Manipur ophiolites, Northeast India: constraints from mineralogical and geochemical characteristics. Geol. J. 52, 415–436.
Singh, T.D., Manikyamba, C., Subramanyam, K.S.V., Ganguly, S., Khelen, A.C., Reddy, N.R., 2018. Mantle heterogeneity, plume-lithosphere interaction at rift controlled ocean-continent transition zone: evidence from trace-PGE geochemistry of Vempalle flows, Cuddapah Basin, India. Geosci. Front. 9, 1809–1827.
Sinha, A.K., Mishra, M., 1992. Emplacement of the ophiolitic mélange along continental collision zone of Indus Suture Zone in Ladakh Himalaya. J. Himal. Geol. 3, 179–189.
Song, X.Y., Keays, R.R., Xiao, L., Qi, H.W., Ihlenfeld, C., 2009. Platinum-group element geochemistry of the continental flood basalts in the Central Emeishan large Igneous Province, SW China. Chem. Geol. 262, 246–261.
Stern, R.J., 2004. Subduction initiation: spontaneous and induced. Earth Planet. Sci. Lett. 226, 275–292.
Thakur, V.C., Misra, D.K., 1984. Tectonic framework of Indus and Shyok Suture zones in eastern Ladakh, NW Himalaya. Tectonophysics 101, 207–220.
Ullah, Z., Li, J.W., Robinson, P.T., Wu, W.W., Khan, A., Dac, N.X., Adam, M.M.A., 2020. Mineralogy and geochemistry of peridotites and chromitites in the Jijal complex ophiolite along the Main Mantle Thrust (MMT or Indus Suture Zone) North Pakistan. Lithos 366–367, 105566.
Uysal, I., Ersoy, E.Y., Karsli, O., Dilek, Y., Burhan Sadiklar, M., Ottley, C.J., Tiepolo, M., Meisel, T., 2012. Coexistence of abyssal and ultra–depleted SSZ type mantle peridotites in a Neo–Tethyan Ophiolite in SW Turkey: Constraints from mineral composition, whole–rock geochemistry (major–race–REE–PGE) and Re–Os isotope systematics. Lithos 132, 50–69.
Whattam, S.A., Stern, R.J., 2011. The 'subduction initiation rule': a key for linking ophiolites, intra-oceanic fore-arcs, and subduction initiation. Contrib. Mineral. Petrol. 162, 1031–1045.
Woelki, D., Regelous, M., Haase, K.M., Romer, R.H.W., Beier, C., 2018. Petrogenesis of boninitic lavas from the Troodos Ophiolite, and comparison with Izu–Bonin–Mariana fore-arc crust. Earth Planet. Sci. Lett. 498, 203–214.
Xiong, F., Yang, J., Robinson, P.T., Gao, J., Chen, Y., Lai, S., 2017. Petrology and geochemistry of peridotites and podiform chromitite in the Xigaze ophiolite, Tibet: implications for a supra-subduction zone origin. J. Asian Earth Sci. 146, 56–75.
Xu, Y., Liu, C.Z., 2019. Subduction-induced fractionated highly siderophile element patterns in fore-arc mantle. Miner. 9 (6), 339. https://doi.org/10.3390/min9060339.
Xu, Y., Liu, J., Xiong, Q., Su, B.X., Scott, J.M., Xu, B., Zhu, D.C., Pearson, D.G., 2020. The complex life cycle of oceanic lithosphere: a study of Yarlung-Zangbo ophiolitic peridotites, Tibet. Geochim. Cosmochim. Acta 277, 175–191.
Yin, A., Harrison, T.M., 2000. Geologic evolution of the Himalayan–Tibetan orogen. Ann. Rev. Earth Planet. Sci. Lett. 28, 211–280.
Yu, H., Xla, B., Mei, H., Guo, L., Ql, L., Tu, X., 2001. Platinum group elements for the mantle peridotites in the Dazhuka ophiolite, Tibet, China. Chin. Sci. Bull. 46, 259–264.

Zaccarini, F., Garuti, G., Pushkarev, E.V., 2011. Unusually PGE-rich chromitite in the Butyrin vein of the Kytlym Uralian-Alaskan complex, Northern Urals, Russia. Can. Mineral. 49, 52–72.

Zaccarini, F., Garuti, G., Pushkarev, E., Thalhammer, O., 2018. Origin of platinum group minerals (PGM) inclusions in chromite deposits of the Urals. Minerals 8 (9), 379.

Zhao, J.J., Zhou, M.F., 2007. Geochemistry of Neoproterozoic mafic intrusions in the Panzhihua district (Sichuan Province, SW China): implications for subduction related metasomatism in the upper mantle. Precambrian Res. 152, 27–47.

Zheng, J., Zhimin, C., Song, X., Wei, A., Liu, J., 2004. Platinum-group elements geochemistry of the Yangliuping magmatic Ni-Cu-PGE sulfide deposit: implications of its Genetic link with the extrusive basalts. J. Ocean Univ. China 3, 93–98.

Zhou, M.F., Sun, M., Keays, R.R., Kerrich, R.W., 1998. Controls on platinum-group elemental distributions of podiform chromitites: a case study of high-Cr and high-Al chromitites from Chinese orogenic belts. Geochim. Cosmochim. Acta 62, 677–688.

Zhou, M.F., Robinson, P.T., Malpas, J., Edwards, S.J., Qi, L., 2005. REE and PGE geochemical constraints on the formation of dunites in the Luobusa ophiolite, Southern Tibet. J. Petrol. 46, 615–639.